

Calibrated Bayesian inference for random fields on large irregular domains using the debiased spatial Whittle likelihood

Thomas Goodwin* Arthur Guillaumin† Matias Quiroz‡ Mattias Villani§
Robert Kohn*

Abstract

Bayesian inference for stationary random fields is computationally demanding. Whittle-type likelihoods in the frequency domain based on the fast Fourier Transform (FFT) have several appealing features: i) low computational complexity of only $\mathcal{O}(n \log n)$, where n is the number of spatial locations, ii) robustness to assumptions of the data-generating process, iii) ability to handle missing data and irregularly spaced domains, and iv) flexibility in modelling the covariance function via the spectral density directly in the spectral domain. It is well known, however, that the Whittle likelihood suffers from bias and low efficiency for spatial data. The debiased Whittle likelihood is a recently proposed alternative with better frequentist properties. We propose a methodology for Bayesian inference for stationary random fields using the debiased spatial Whittle likelihood, with an adjustment from the composite likelihood literature. The adjustment is shown to give a well-calibrated Bayesian posterior as measured by coverage properties of credible sets, without sacrificing the quasi-linear computation time. We apply the method to simulated data and two real datasets.

Keywords: Bayesian calibration, Composite likelihood, Frequency domain.

1 Introduction

The collection and analysis of spatial data is crucial in many fields, such as geology (Cressie, 1989; Matheron, 1963), climatology (Berliner et al., 2000; Hrafnkelsson and Cressie, 2003), and epidemiology (Tolbert et al., 2000; Best et al., 2001). Technological advancements make it possible to cheaply collect and store large amounts of spatial data. It is therefore important to develop models and estimation methods that can handle large-scale spatial data in a computationally feasible way.

Computing the likelihood for Gaussian random fields involves solving computationally demanding large systems of equations. Approximate methods like those in Anitescu et al.

*School of Economics, University of New South Wales.

†School of Mathematical Sciences, Queen Mary University of London.

‡School of Mathematical and Physical Sciences, University of Technology Sydney.

§Department of Statistics, Stockholm University.

(2017) and Stein et al. (2013) focus on estimating equation approaches to side-step expensive matrix computations via optimization and stochastic approximations, respectively. Stroud et al. (2017) and Guinness and Fuentes (2017) use circulant embedding techniques. Sidén et al. (2021) use fast preconditioned conjugate gradient solvers. The class of stochastic partial differential equation (SPDE) models in Lindgren et al. (2011) approximates Gaussian random fields with the Matérn covariance kernel by sparse and numerically efficient Gaussian Markov random fields (Rue and Held, 2005). Finally, so-called Vecchia approximations utilizing conditional independence (given a number of neighbors) of the field have been proposed to approximate the likelihood (Vecchia, 1988; Katzfuss and Guinness, 2021).

Another line of research uses the Whittle likelihood (Whittle, 1954) to approximate the likelihood in the spectral domain (Gelfand et al., 2010). Whittle-type likelihoods have several appealing features: i) low computational complexity of only $\mathcal{O}(n \log n)$ from using the fast Fourier Transform (FFT), where n is the number of spatial locations (Gelfand et al., 2010), ii) robustness to assumptions of the data-generating process, iii) easy handling of missing data and irregularly spaced domains (Fuentes, 2007; Matsuda and Yajima, 2009), and iv) flexibility in modelling the covariance function directly in the spectral domain via the spectral density. Moreover, Whittle-type likelihoods open up for using efficient Markov chain Monte Carlo subsampling techniques (Quiroz et al., 2019, 2021) in the frequency domain to further speed up posterior sampling algorithms both for univariate (Salomone et al., 2020) and multivariate (Villani et al., 2024) data. The Whittle likelihood was initially developed for linear Gaussian models but has been extended to more general settings (Shao and Wu, 2007).

When used for time series data, the Whittle approximation is usually quite accurate with a small bias for the corresponding maximum likelihood estimator (MLE). Exceptions might occur due to a high dynamic range (the ratio between the maximum and minimum of the power spectrum), which can result in significant leakage, or due to not accounting for aliasing (Sykulski et al., 2019). In contrast, for two-dimensional (2D) data, for example, spatial data, the bias of the MLE based on the Whittle likelihood is substantial. Guyon (1982) and Kent and Mardia (1996) prove that the bias incurred by the Whittle approximation is of the same order as the standard error in 2D, and that the bias is dominant for 3D spatial data; see also Dahlhaus and Künsch (1987).

Guillaumin et al. (2022) propose a debiased Whittle MLE by replacing the spectral density in the Whittle likelihood with the expected periodogram. They prove that their estimator has the same $\mathcal{O}(n^{-1/2})$ efficiency as the standard MLE in the time/space domain, regardless of the dimension of the lattice. However, because the debiased Whittle is a pseudo-likelihood, constructing a Bayesian posterior distribution based on the debiased Whittle likelihood is not guaranteed to be well-calibrated in the sense of Modrák et al. (2023), i.e. credible sets may not have the intended coverage.

Our paper makes the following contributions. We demonstrate that a Bayesian posterior distribution for the covariance kernel parameters based on the debiased Whittle likelihood can be badly calibrated (Modrák et al., 2023) and will, therefore, not convey proper uncertainty

quantification of the parameters. Using ideas from the composite likelihood literature in Ribatet et al. (2012), two alternative adjustments to the debiased Whittle posterior are presented. The adjusted debiased Whittle posteriors are empirically shown to be well-calibrated in a simulation study. Two real data applications are used to demonstrate the proposed method and to compare it against the standard Whittle posterior and the unadjusted debiased Whittle posterior.

The rest of the article is organized as follows. Section 2 reviews Whittle-type approximations to the exact Gaussian random fields likelihood and demonstrates that they result in poorly approximated posteriors. Section 3 reviews the concept of posterior calibration and proposes two methods for calibrating the debiased Whittle posterior, which are subsequently validated in a simulation study. Section 4 demonstrates our method on two challenging large-scale datasets. Section 5 concludes and outlines future research.

2 Whittle-type likelihood approximations

In this section, we review Whittle-type likelihood approximations that can be used to circumvent the computational burden of the exact Gaussian likelihood. In particular, we discuss how the debiased spatial Whittle likelihood addresses several shortcomings of the standard Whittle likelihood.

2.1 The exact Gaussian likelihood

Let $X(\mathbf{s}) \in \mathbb{R}$ be a finite variance, zero-mean random field indexed by the spatial location $\mathbf{s} \in \mathbb{R}^d$ where $d \geq 1$ is a positive integer. Assume $X(\mathbf{s})$ is stationary — but not necessarily isotropic — and denote its covariance function by $c_{\boldsymbol{\theta}}(\mathbf{u})$, $\mathbf{u} \in \mathbb{R}^d$, which is governed by some unknown parameters $\boldsymbol{\theta} \in \boldsymbol{\Theta} \subset \mathbb{R}^p$ and is assumed to be square-summable. One of the most widely used covariance kernels is the isotropic Matérn kernel,

$$c_{\boldsymbol{\theta}}(\mathbf{u}) = \sigma^2 \frac{2^{1-\nu}}{\Gamma(\nu)} \left(\sqrt{2\nu} \frac{\|\mathbf{u}\|}{\rho} \right)^{\nu} B_{\nu} \left(\sqrt{2\nu} \frac{\|\mathbf{u}\|}{\rho} \right), \quad (1)$$

where $\Gamma(\cdot)$ and $B_{\nu}(\cdot)$ are, respectively, the Gamma function and the Bessel function of the second kind, and $\|\cdot\|$ is the Euclidean norm. The three parameters in $\boldsymbol{\theta} = (\rho, \sigma, \nu)^{\top}$ are the range ρ , amplitude σ and smoothness ν .

Suppose that the observed random field $X_{\mathbf{s}}$ is sampled on an orthogonal rectangular grid $\mathcal{G}_{\mathbf{n}}$ with size $\mathbf{n} = (n_1, \dots, n_d) \in (\mathbb{N}^+)^d$ and $|\mathbf{n}| = \prod_{i=1}^d n_i$ denoting the total number of grid points. Furthermore, we denote the spacing between observations for each dimension as $\boldsymbol{\delta} = (\delta_1, \dots, \delta_d)$ with $|\boldsymbol{\delta}| = \prod_{i=1}^d \delta_i$. Throughout the simulations and real data examples, without loss of generality, we assume that the grid has a unit step size in all dimensions, i.e. $\delta_1 = \dots = \delta_d = 1$. Our methodology can also accommodate missing data and irregular sampling domains/boundaries, see below.

Let $p(\boldsymbol{\theta})$ denote the prior of the kernel parameters. Exploring the posterior distribution $p(\boldsymbol{\theta}|X_{\mathbf{s}}) \propto \mathcal{L}(\boldsymbol{\theta})p(\boldsymbol{\theta})$ requires computing the likelihood function $\mathcal{L}(\boldsymbol{\theta})$. We use the term “likelihood” to refer to both the log-likelihood and likelihood, with the intended meaning clear from the context. The exact likelihood for Gaussian random fields is

$$\ell_{\text{true}}(\boldsymbol{\theta}) = -\frac{|\mathbf{n}|}{2} \log(2\pi) - \frac{1}{2} \log \det\{\boldsymbol{\Sigma}(\boldsymbol{\theta})\} - \frac{1}{2} X_{\mathbf{s}}^{\top} \boldsymbol{\Sigma}^{-1}(\boldsymbol{\theta}) X_{\mathbf{s}}, \quad (2)$$

where $\boldsymbol{\Sigma}(\boldsymbol{\theta})$ is the $|\mathbf{n}| \times |\mathbf{n}|$ covariance matrix corresponding to $c_{\boldsymbol{\theta}}(\mathbf{u})$ and $\det\{\boldsymbol{\Sigma}(\boldsymbol{\theta})\}$ is the determinant of the covariance matrix. Evaluation of the likelihood is computationally challenging since $\det\{\boldsymbol{\Sigma}(\boldsymbol{\theta})\}$ is $\mathcal{O}(|\mathbf{n}|^3)$ in general, or $\mathcal{O}(|\mathbf{n}|^{5/2})$ in structured cases (Sowell, 1989; Akaike, 1973). Furthermore, this likelihood is restrictive as it assumes the data-generating process is Gaussian, which may not be appropriate when modelling real data (Guilleminot, 2020).

2.2 The Whittle likelihood

For any stationary random field, Bochner’s theorem (Brockwell and Davis, 2009) guarantees that there exists a spectral distribution function $F_{\boldsymbol{\theta}}(\boldsymbol{\omega})$ such that

$$c_{\boldsymbol{\theta}}(\mathbf{u}) = \mathbb{E}_{\boldsymbol{\theta}}[X_{\mathbf{s}} X_{\mathbf{s}+\mathbf{u}}] = \int_{\mathbb{R}^d} \exp(i\boldsymbol{\omega} \cdot \mathbf{u}) dF_{\boldsymbol{\theta}}(\boldsymbol{\omega}), \quad \forall \mathbf{u} \in \mathbb{R}^d,$$

where the expectation is for a fixed $\boldsymbol{\theta}$, $\boldsymbol{\omega} \in \mathbb{R}^d$ is a frequency vector, \cdot is the dot product and we assume that $F_{\boldsymbol{\theta}}(\boldsymbol{\omega})$ is absolutely continuous, such that it admits a spectral density function, $f_{\boldsymbol{\theta}}(\boldsymbol{\omega}) = \int_{\mathbb{R}^d} c_{\boldsymbol{\theta}}(\mathbf{u}) \exp(-i\boldsymbol{\omega} \cdot \mathbf{u}) d\mathbf{u}$. The *aliased* spectral density $f_{\boldsymbol{\theta},\delta}(\boldsymbol{\omega})$ of the sampled random field is,

$$f_{\boldsymbol{\theta},\delta}(\boldsymbol{\omega}) = \sum_{\mathbf{u} \in \mathbb{Z}^d} f_{\boldsymbol{\theta}}\left(\boldsymbol{\omega} + \frac{2\pi\mathbf{u}}{\delta}\right), \quad \boldsymbol{\omega} \in \mathbb{R}^d. \quad (3)$$

The periodogram of the sampled random field is given by

$$I_{\mathbf{n}}(\boldsymbol{\omega}) = \frac{(2\pi)^{-d} |\delta|}{\sum_{\mathbf{s} \in \mathcal{G}_{\mathbf{n}}} g_{\mathbf{s}}^2} \left| \sum_{\mathbf{s} \in \mathcal{G}_{\mathbf{n}}} g_{\mathbf{s}} X_{\mathbf{s}} \exp(-i\boldsymbol{\omega} \cdot \mathbf{s}) \right|^2, \quad \boldsymbol{\omega} \in \mathbb{R}^d, \quad (4)$$

where $g_{\mathbf{s}}$, $\forall \mathbf{s} \in \mathcal{G}_{\mathbf{n}}$, is a masking grid which takes value 0 if an observation is missing, and 1 otherwise. Moreover, the masking grid $g_{\mathbf{s}}$ also accommodates tapering, which can take values in the interval $[0, 1]$, with 0 still indicating a missing value. Note that in the case of a fully observed grid with no tapering, the denominator in (4) reduces to $|\mathbf{n}|$. Guinness and Fuentes (2017); Stroud et al. (2017) use procedures that impute missing observations via circulant embedding, which may not be appropriate when the data violates the Gaussian assumption. Instead, the debiased Whittle handles missing observations and irregular sampling domains via the modulation values $g_{\mathbf{s}}$ (Parzen, 1963). The periodogram in (4) is computed on a

multidimensional grid of Fourier frequencies

$$\Omega_{\mathbf{n}} = \prod_{j=1}^d \left\{ \frac{2\pi k}{\delta_j n_j} : k = 0, \dots, n_j - 1 \right\}.$$

The periodogram can be efficiently evaluated, regardless of missing observations or use of tapering, at a computation cost of $\mathcal{O}(|\mathbf{n}|\log|\mathbf{n}|)$ operations via the FFT. The Whittle likelihood is a computationally efficient approximation to the Gaussian likelihood that relies on the following asymptotic result (Whittle, 1954)

$$I_{\mathbf{n}}(\boldsymbol{\omega}) \stackrel{\text{ind}}{\sim} \text{Exp}\{f_{\boldsymbol{\theta},\delta}(\boldsymbol{\omega})\}, \quad \boldsymbol{\omega} \in \Omega_{\mathbf{n}},$$

where $\text{Exp}(\lambda)$ is an exponential distribution parameterized by its mean λ . The Whittle likelihood is then

$$\ell_W(\boldsymbol{\theta}) = -\frac{1}{2} \sum_{\boldsymbol{\omega} \in \Omega_{\mathbf{n}}} \left\{ \log f_{\boldsymbol{\theta},\delta}(\boldsymbol{\omega}) + \frac{I_{\mathbf{n}}(\boldsymbol{\omega})}{f_{\boldsymbol{\theta},\delta}(\boldsymbol{\omega})} \right\}. \quad (5)$$

Guyon (1982) and Kent and Mardia (1996) studied the accuracy of the Whittle likelihood approximation to the exact likelihood in (2) and prove that

$$|\ell_{\text{true}}(\boldsymbol{\theta}) - \ell_W(\boldsymbol{\theta})| = \mathcal{O}_P(|\mathbf{n}|/n_1) \quad (6)$$

as $n_1 \rightarrow \infty$, where n_1 is the number of points on the smallest side of the lattice. Denote $\hat{\boldsymbol{\theta}}_W$ as the maximum likelihood estimator of $\boldsymbol{\theta}$ using the likelihood in (5). From (6) it can be shown that bias of $\hat{\boldsymbol{\theta}}_W$ is of the same order as the standard error when $d = 2$, and for $d > 2$ the bias is of larger order than the standard error. Hence, for $d \geq 2$, $\hat{\boldsymbol{\theta}}_W$ is not an efficient estimator. For tapered data, Dahlhaus and Künsch (1987) show that $\hat{\boldsymbol{\theta}}_W$ is efficient for $d = 2, 3$. Despite the efficiency of $\hat{\boldsymbol{\theta}}_W$ for tapered data, the rate of convergence is of the same order as the smallest side n_1 . This is a drawback of the standard Whittle approximation as the bias of the MLE and its likelihood approximation is limited by the smallest side. Simulation studies suggest that the bias of $\hat{\boldsymbol{\theta}}_W$ decreases slowly with respect to the grid size, see Figures 1 and 2 in Guillaumin et al. (2022).

To assess the approximation of the likelihood function over Θ or around $\hat{\boldsymbol{\theta}}_W$, we are interested in the relative order of error, i.e.

$$\left| \frac{\ell_{\text{true}}(\boldsymbol{\theta}) - \ell_W(\boldsymbol{\theta})}{\ell_{\text{true}}(\boldsymbol{\theta})} \right| = \mathcal{O}_P(1/n_1). \quad (7)$$

The above equation illustrates the (probabilistic) convergence of the Whittle likelihood to the exact likelihood. From (7), we conclude that the relative error of the Whittle likelihood goes to zero (in probability) for square grids (which increase in all directions).

To illustrate the poor posterior approximation based on the standard Whittle likelihood for spatial data, we simulate data on a square grid of $n = (64, 64)$ from a Gaussian random

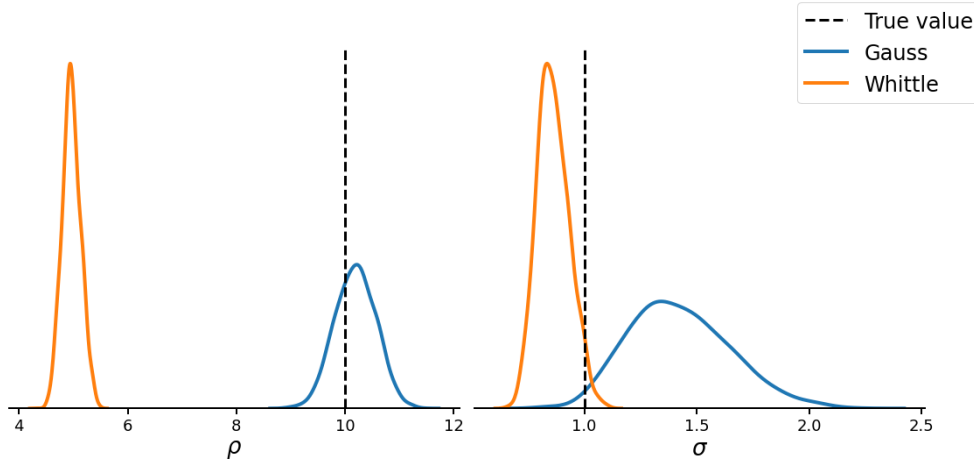


Figure 1: Kernel density estimates of the marginal posteriors based on different likelihoods (exact Gaussian, standard Whittle) for a simulated data example with a squared-exponential kernel with grid size $n = (64, 64)$.

field with the isotropic Matérn kernel in (1). We set the true values $\rho = 10$ and $\sigma = 1$, and fix $\nu = \infty$, which is not estimated. This corresponds to the squared-exponential kernel. Figure 1 shows the marginal posterior density of ρ and σ from a non-informative prior for the exact Gaussian likelihood and the Whittle approximation. As seen in Figure 1, the Whittle posteriors are poor approximations of the posteriors from the exact Gaussian likelihood, particularly for the ρ parameter.

The following subsection presents the recently proposed debiased Whittle likelihood (Sykulski et al., 2019; Guillaumin et al., 2022) and demonstrates that it requires modification to ensure well-calibrated Bayesian inference in terms of its posterior coverage properties.

2.3 The debiased Whittle likelihood

The debiased Whittle likelihood in Sykulski et al. (2019) for time series improves on the Whittle likelihood by reducing the bias. This is extended to domains of higher dimensions in Guillaumin et al. (2022), e.g. for the analysis of spatial or spatiotemporal random processes. The debiased spatial Whittle likelihood is

$$\ell_{dW}(\boldsymbol{\theta}) = -\frac{1}{2} \sum_{\boldsymbol{\omega} \in \Omega_{\mathbf{n}}} \left\{ \log \bar{I}_{\mathbf{n}}(\boldsymbol{\omega}; \boldsymbol{\theta}) + \frac{I_{\mathbf{n}}(\boldsymbol{\omega})}{\bar{I}_{\mathbf{n}}(\boldsymbol{\omega}; \boldsymbol{\theta})} \right\}, \quad (8)$$

where,

$$\bar{I}_{\mathbf{n}}(\boldsymbol{\omega}; \boldsymbol{\theta}) = \mathbb{E}_{\boldsymbol{\theta}} [I_{\mathbf{n}}(\boldsymbol{\omega})], \quad \forall \boldsymbol{\omega} \in \Omega_{\mathbf{n}}, \quad (9)$$

is the expected periodogram. Maximization of (8) over Θ defines the debiased Whittle maximum likelihood estimator

$$\hat{\boldsymbol{\theta}}_{dW} = \arg \max_{\boldsymbol{\theta} \in \Theta} \ell_{dW}(\boldsymbol{\theta}).$$

Equation (8) shows that the debiased Whittle likelihood replaces the spectral density in the Whittle likelihood in (5) with the expected periodogram. The expected periodogram in (9) can be expressed as a convolution

$$\bar{I}_{\mathbf{n}}(\boldsymbol{\omega}; \boldsymbol{\theta}) = \{f_{\boldsymbol{\theta}, \delta} * \mathcal{F}_{\mathbf{n}}\}(\boldsymbol{\omega}) = \int_{\mathcal{T}} f_{\boldsymbol{\theta}, \delta}(\boldsymbol{\omega} - \boldsymbol{\omega}') \mathcal{F}_{\mathbf{n}, \delta}(\boldsymbol{\omega}') d\boldsymbol{\omega}', \quad (10)$$

where $\mathcal{T} = [0, 2\pi/\delta_1) \times \cdots \times [0, 2\pi/\delta_d)$, between the spectral density of the process and the multi-dimensional *modified* Féjer kernel

$$\mathcal{F}_{\mathbf{n}}(\boldsymbol{\omega}) = \frac{(2\pi)^{-d} |\delta|}{\sum_{\mathbf{s} \in \mathcal{G}_{\mathbf{n}}} g_{\mathbf{s}}^2} \left| \sum_{\mathbf{s} \in \mathcal{G}_{\mathbf{n}}} g_{\mathbf{s}} \exp(-i\boldsymbol{\omega} \cdot \mathbf{s}) \right|^2, \quad \boldsymbol{\omega} \in \mathbb{R}^d.$$

In the case of a fully observed domain with no tapering, this kernel becomes the multidimensional rectangular Féjer kernel, i.e. a separable product of one-dimensional Féjer kernels.

The debiased Whittle likelihood corresponds to the model

$$I_{\mathbf{n}}(\boldsymbol{\omega}) \stackrel{\text{ind}}{\sim} \text{Exp} \{ \bar{I}_{\mathbf{n}}(\boldsymbol{\omega}; \boldsymbol{\theta}) \}, \quad \boldsymbol{\omega} \in \Omega_{\mathbf{n}}. \quad (11)$$

Specifically, it ignores potential dependencies of the periodogram between distinct Fourier frequencies and, as such, can be considered misspecified and follows the framework of composite likelihoods (Varin et al., 2011). Guillaumin et al. (2022) note that the estimator $\hat{\boldsymbol{\theta}}_{\text{dW}}$ fits the methodology of estimating equations in Heyde (1997), since $\text{E}_{\boldsymbol{\theta}}[\nabla_{\boldsymbol{\theta}} \ell_{\text{dW}}(\boldsymbol{\theta})] = \mathbf{0}$, where $\nabla_{\boldsymbol{\theta}}$ denotes the gradient with respect to $\boldsymbol{\theta}$, i.e. $\nabla_{\boldsymbol{\theta}} \ell_{\text{dW}}(\boldsymbol{\theta})$ is the score function. Guillaumin et al. (2022) also prove that the debiased Whittle MLE has the same asymptotic efficiency as the time/space MLE, a result that holds for any dimension d of the random field.

The implementation of the expected periodogram in (10) can take advantage of the FFT and is therefore an $\mathcal{O}(|\mathbf{n}| \log |\mathbf{n}|)$ operation. This holds for any d , regardless of missing data or irregular domain patterns. The expected periodogram can directly account for finite sampling effects, such as aliasing and spectral leakage. The quantity $\bar{I}_{\mathbf{n}}(\boldsymbol{\omega}; \boldsymbol{\theta})$ is computed via the FFT of the discretely sampled theoretical covariance function combined with, in the case of fully observed grids, a multidimensional triangular kernel (Percival and Walden, 1993). Thus, the expected periodogram accounts for aliasing via discrete sampling of the covariance function and spectral leakage by inclusion of the triangular kernel. This is significant as the alternative of evaluating $f_{\boldsymbol{\theta}, \delta}(\boldsymbol{\omega})$ in (3) as required in the standard Whittle likelihood estimation may be difficult (Sykulski et al., 2019; Guillaumin et al., 2022). For example, the aliased spectral density $f_{\boldsymbol{\theta}, \delta}(\boldsymbol{\omega})$ seldom has an analytical form and is usually approximated in practice (Gelfand et al. 2010, Chapter 5) by truncation of the infinite sum in (3) via ‘wrapping’ contributions from $f_{\boldsymbol{\theta}}(\boldsymbol{\omega})$ for frequencies above the Nyquist frequency. This requires additional methods to account for aliasing, spectral leakage, missing data, and irregular sampling domains. All of these are automatically accounted for when computing $\bar{I}_{\mathbf{n}}(\boldsymbol{\omega}; \boldsymbol{\theta})$.

In the case of fully observed grids, Guillaumin et al. (2022) use Fejér’s theorem (Körner,

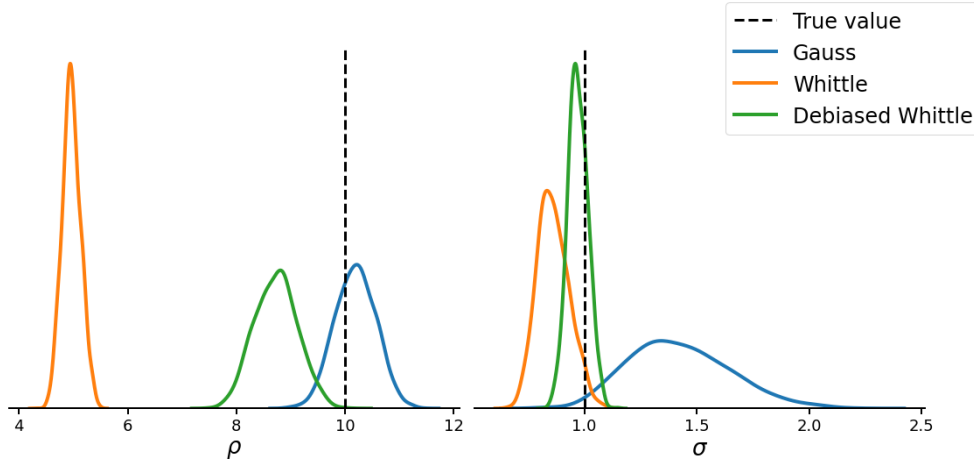


Figure 2: Kernel density estimates of the marginal posteriors based on different likelihoods (exact Gaussian, standard Whittle, debiased Whittle) for a simulated data example with a squared-exponential kernel with grid size $n = (64, 64)$.

1988) to show that

$$\bar{I}_{\mathbf{n}}(\boldsymbol{\omega}; \boldsymbol{\theta}) = \mathbb{E}_{\boldsymbol{\theta}} [I_{\mathbf{n}}(\boldsymbol{\omega})] \xrightarrow{\mathbf{n} \rightarrow \infty} f_{\boldsymbol{\theta}, \delta}(\boldsymbol{\omega}),$$

if $f_{\boldsymbol{\theta}, \delta}$ is continuous, where $\mathbf{n} \rightarrow \infty$ denotes $n_i \rightarrow \infty$ for $i = 1, \dots, d$. Hence, there is an asymptotic equivalence between the debiased Whittle and standard Whittle likelihoods. For more details on the expected periodogram and its computation, see Guillaumin et al. (2022).

Figure 2 displays the marginal posteriors based on the three likelihoods (exact Gaussian, standard Whittle, debiased Whittle) with the same simulated data as in Figure 1. While the bias is reduced for the debiased Whittle posterior, the posterior uncertainty for σ — as is the case with the standard Whittle — is small compared to the exact Gaussian posterior, a common phenomenon for composite likelihoods (Ribatet et al., 2012). The next section shows how to adjust the posterior to obtain a better calibrated uncertainty quantification.

3 Calibrating the debiased spatial Whittle posterior

In this section, we investigate calibration methods to allow for valid Bayesian inference using the debiased spatial Whittle likelihood. We formally define valid posteriors, following Monahan and Boos (1992), and then propose curvature adjustments based on Ribatet et al. (2012). We present simulation studies that demonstrate the ability of the proposed methodology to leverage the debiased spatial Whittle likelihood for Bayesian inference.

3.1 Well-calibrated posteriors

We follow Monahan and Boos (1992) and define valid posteriors based on coverage properties of posterior sets. Assume the data are generated from the model $X \sim p(X_s | \boldsymbol{\theta})$ and suppose

$\mathcal{L}(\boldsymbol{\theta}; X_{\mathbf{s}})$ is the quasi-likelihood of interest, and we compute the quasi-posterior from

$$\tilde{p}(\boldsymbol{\theta}|X_{\mathbf{s}}) = \frac{\mathcal{L}(\boldsymbol{\theta}; X_{\mathbf{s}})p(\boldsymbol{\theta})}{\tilde{p}(X_{\mathbf{s}})}, \quad \tilde{p}(X_{\mathbf{s}}) = \int_{\Theta} \mathcal{L}(\boldsymbol{\theta}; X_{\mathbf{s}})p(\boldsymbol{\theta})d\boldsymbol{\theta}. \quad (12)$$

Note that (12) corresponds to the Bayesian paradigm only when the likelihood comes from the data-generating process, i.e. $\mathcal{L}(\boldsymbol{\theta}; X_{\mathbf{s}}) = p(X_{\mathbf{s}}|\boldsymbol{\theta})$ and then

$$\tilde{p}(\boldsymbol{\theta}|X_{\mathbf{s}}) = p(\boldsymbol{\theta}|X_{\mathbf{s}}) \text{ and } \tilde{p}(X_{\mathbf{s}}) = p(X_{\mathbf{s}}) = \int_{\Theta} p(X_{\mathbf{s}}|\boldsymbol{\theta})p(\boldsymbol{\theta})d\boldsymbol{\theta}.$$

Define $\tilde{K}_{\alpha}(X_{\mathbf{s}})$ as a posterior coverage set function of level α if, for every $X_{\mathbf{s}}$,

$$\Pr\{\boldsymbol{\theta} \in \tilde{K}_{\alpha}(X_{\mathbf{s}})|X_{\mathbf{s}}\} = \alpha, \quad (X_{\mathbf{s}} \text{ conditioned upon}), \quad (13)$$

where the coverage set $\tilde{K}_{\alpha}(X_{\mathbf{s}})$ is determined from the quasi-posterior $\tilde{p}(\boldsymbol{\theta}|X_{\mathbf{s}})$ for a given $X_{\mathbf{s}}$. Similarly, $K_{\alpha}(X_{\mathbf{s}})$ denotes a posterior coverage set function when the set is determined from the posterior $p(\boldsymbol{\theta}|X_{\mathbf{s}})$. A simple example of a posterior coverage set function is a $1 - \alpha$ highest posterior density (HPD) interval for a one-dimensional parameter. The quasi-posterior $\tilde{p}(\boldsymbol{\theta}|X_{\mathbf{s}})$ is said to be valid by coverage if, for every α ,

$$\Pr\{\boldsymbol{\theta} \in \tilde{K}_{\alpha}(X_{\mathbf{s}})\} = \alpha, \quad (X_{\mathbf{s}} \text{ is random}), \quad (14)$$

where the probability is now with respect to the joint distribution $p(X_{\mathbf{s}}, \boldsymbol{\theta}) = p(X_{\mathbf{s}}|\boldsymbol{\theta})p(\boldsymbol{\theta})$. Note the similarity to the classical statistical coverage, however, the sampling distribution of $X_{\mathbf{s}}$ is averaged over the prior (instead of keeping the parameter at its true value). When the likelihood comes from the data-generating process ($\mathcal{L}(\boldsymbol{\theta}; X_{\mathbf{s}}) = p(X_{\mathbf{s}}|\boldsymbol{\theta})$), the posterior is valid by coverage since

$$\begin{aligned} \Pr\{\boldsymbol{\theta} \in K_{\alpha}(X_{\mathbf{s}})\} &= \int_{X_{\mathbf{s}}} \int_{\boldsymbol{\theta} \in K_{\alpha}(X_{\mathbf{s}})} p(X_{\mathbf{s}}, \boldsymbol{\theta})d\boldsymbol{\theta}dX_{\mathbf{s}} \\ &= \int_{X_{\mathbf{s}}} \int_{\boldsymbol{\theta} \in K_{\alpha}(X_{\mathbf{s}})} p(X_{\mathbf{s}})p(\boldsymbol{\theta}|X_{\mathbf{s}})d\boldsymbol{\theta}dX_{\mathbf{s}} \\ &= \int_{X_{\mathbf{s}}} p(X_{\mathbf{s}}) \left(\int_{\boldsymbol{\theta} \in K_{\alpha}(X_{\mathbf{s}})} p(\boldsymbol{\theta}|X_{\mathbf{s}})d\boldsymbol{\theta} \right) dX_{\mathbf{s}} \\ &= \int_{X_{\mathbf{s}}} p(X_{\mathbf{s}})\alpha dX_{\mathbf{s}} \\ &= \alpha, \end{aligned}$$

using the definition of a posterior coverage set function in (13) (with K in place of \tilde{K}). Monahan and Boos (1992) devise a method to test the validity of (14), see Section 3.5.

We are interested in the case when $\mathcal{L}(\boldsymbol{\theta}; X_{\mathbf{s}})$ differs from $p(X_{\mathbf{s}}|\boldsymbol{\theta})$, specifically when the debiased spatial Whittle likelihood in (8) is used in place of the intractable Gaussian random

field likelihood in (2). Section 3.5 demonstrates that the posterior based on the debiased spatial Whittle likelihood is not valid by coverage (and neither is the standard Whittle likelihood). We now turn to adjusting the approximate posterior based on ideas from the composite likelihood literature. The resulting adjustments are shown to dramatically improve its validity by coverage.

3.2 Posterior adjustments

Ribatet et al. (2012) propose an asymptotic curvature adjustment for composite likelihoods. The framework is closely related to maximum likelihood inference in misspecified models (White, 1982). This curvature adjustment is inspired by the Bernstein Von-Mises theorem (Van der Vaart, 2000), which loosely states that the posterior converges to the asymptotic sampling distribution of the MLE. See Kleijn and van der Vaart (2012) for the Bernstein Von-Mises theorem in the case of misspecified models. Thus, the curvature adjustment corrects the variance of a composite posterior to equal (asymptotically) the variance of its corresponding maximum composite likelihood estimator (MCLE). In our case, Guillaumin et al. (2022) show that for finite grid sizes, the debiased spatial Whittle likelihood is a composite likelihood (Varin et al., 2011; Bevilacqua and Gaetan, 2015) and fits within the framework of estimating equations (Heyde, 1997). We briefly review how to perform these adjustments for composite likelihoods.

Let $\ell_c^{\text{tot}}(\boldsymbol{\theta})$ denote the composite likelihood of a sample with n observations, which assuming independence decomposes as

$$\ell_c^{\text{tot}}(\boldsymbol{\theta}) = \sum_{i=1}^n \ell_c(\boldsymbol{\theta}; y_i), \quad (15)$$

where $\ell_c(\boldsymbol{\theta}; y_i)$ denote the individual likelihood contributions for observations y_i , $i = 1, \dots, n$. In the analogy to our case, the contributions correspond to the summands (multiplied by -0.5) in (5) and (8) with y_i being the periodogram of the i th frequency and $n = |\mathbf{n}|$. We use $\ell_c(\boldsymbol{\theta})$ as a compact notation for $\ell_c(\boldsymbol{\theta}; y)$. Let $\hat{\boldsymbol{\theta}}_c$ be the maximum composite likelihood estimator (MCLE) obtained by maximizing (15). Moreover, denoting the true parameter as $\boldsymbol{\theta}_0$ and the Hessian with respect to $\boldsymbol{\theta}$ as $\nabla_{\boldsymbol{\theta}}^2 \ell_c(\boldsymbol{\theta})$, let

$$\mathbf{H}(\boldsymbol{\theta}_0) = -\mathbb{E}_{\boldsymbol{\theta}} \left[\nabla_{\boldsymbol{\theta}}^2 \ell_c(\boldsymbol{\theta}) \big|_{\boldsymbol{\theta}=\boldsymbol{\theta}_0} \right], \quad \mathbf{J}(\boldsymbol{\theta}_0) = \text{Var}_{\boldsymbol{\theta}} \left[\nabla_{\boldsymbol{\theta}} \ell_c(\boldsymbol{\theta}) \big|_{\boldsymbol{\theta}=\boldsymbol{\theta}_0} \right],$$

denote the Fisher information matrix and the covariance of the score function, respectively. For proper likelihoods, $\mathbf{H}(\boldsymbol{\theta}_0) = \mathbf{J}(\boldsymbol{\theta}_0)$ (under the usual regularity conditions) and the asymptotic distribution of the MLE $\hat{\boldsymbol{\theta}}$ is

$$\sqrt{|\mathbf{n}|} \mathbf{H}(\boldsymbol{\theta}_0)^{1/2} (\hat{\boldsymbol{\theta}} - \boldsymbol{\theta}_0) \xrightarrow{d} \mathbf{N}(\mathbf{0}, \mathbf{I}).$$

For composite likelihoods on the other hand, $\mathbf{H}(\boldsymbol{\theta}_0) \neq \mathbf{J}(\boldsymbol{\theta}_0)$, and the asymptotic distribution

of the MCLE $\hat{\boldsymbol{\theta}}_c$ is

$$\sqrt{|\mathbf{n}|}\mathbf{G}(\boldsymbol{\theta}_0)^{1/2}(\hat{\boldsymbol{\theta}}_c - \boldsymbol{\theta}_0) \xrightarrow{d} \mathbf{N}(\mathbf{0}, \mathbf{I}). \quad (16)$$

where $\mathbf{G}(\boldsymbol{\theta})^{1/2}$ is the matrix square root of the so-called ‘sandwich’ variance matrix (Varin et al., 2011), defined as

$$\mathbf{G}(\boldsymbol{\theta}) = \mathbf{H}(\boldsymbol{\theta})\mathbf{J}^{-1}(\boldsymbol{\theta})\mathbf{H}(\boldsymbol{\theta}).$$

For large enough $|\mathbf{n}|$, it can be shown (Appendix A of Ribatet et al., 2012) that the composite posterior $\pi_c(\boldsymbol{\theta}) \propto \exp(\ell_c^{\text{tot}}(\boldsymbol{\theta}))p(\boldsymbol{\theta})$ is approximately

$$\pi_c(\boldsymbol{\theta}) \sim \mathbf{N}(\boldsymbol{\theta}_0, |\mathbf{n}|^{-1}\mathbf{H}^{-1}(\boldsymbol{\theta}_0)). \quad (17)$$

We see that there is a mismatch in the posterior covariance of (17) to what we expect if the posterior distribution converged to the sampling distribution of the MCLE, i.e. $|\mathbf{n}|^{-1}\mathbf{G}^{-1}(\boldsymbol{\theta}_0)$ (Kleijn and van der Vaart, 2012). The composite marginal posterior distributions of the parameters tend to have too small posterior variance compared to the posterior; see Figure 1 of Ribatet et al. (2012). The idea in Ribatet et al. (2012) is to rescale the samples from the composite posterior to adjust for this as follows.

Define the asymptotically curvature-adjusted composite likelihood as

$$\ell_{\text{curv}}^{\text{tot}}(\boldsymbol{\theta}) = \ell_c^{\text{tot}}(\boldsymbol{\theta}^*), \quad \boldsymbol{\theta}^* = \hat{\boldsymbol{\theta}}_c + \mathbf{C}(\boldsymbol{\theta} - \hat{\boldsymbol{\theta}}_c),$$

where \mathbf{C} is a positive semi-definite adjustment matrix such that

$$\mathbf{C}^\top \mathbf{H}(\boldsymbol{\theta}_0) \mathbf{C} = \mathbf{H}(\boldsymbol{\theta}_0) \mathbf{J}(\boldsymbol{\theta}_0)^{-1} \mathbf{H}(\boldsymbol{\theta}_0).$$

Ribatet et al. (2012) propose $\mathbf{C} = \mathbf{M}^{-1} \mathbf{M}_A$ where $\mathbf{M}_A^\top \mathbf{M}_A = \mathbf{G}(\boldsymbol{\theta}_0)$ and $\mathbf{M}^\top \mathbf{M} = \mathbf{H}(\boldsymbol{\theta}_0)$. The purpose of this adjustment is for $\ell_{\text{curv}}^{\text{tot}}(\boldsymbol{\theta})$ at $\hat{\boldsymbol{\theta}}_c$ to match the curvature of the large-sample density of $\hat{\boldsymbol{\theta}}_c$ (recall the Bernstein Von-Mises theorem for misspecified models). As a consequence, the curvature adjustment changes the location of any local maxima except the global maximum at $\hat{\boldsymbol{\theta}}_c$, which may not be appropriate if the posterior is multi-modal. The resulting asymptotic distribution of the curvature adjusted posterior $\pi_{\text{curv}}(\boldsymbol{\theta}) \propto \exp(\ell_{\text{curv}}^{\text{tot}}(\boldsymbol{\theta}))p(\boldsymbol{\theta})$ (see Appendix A of Ribatet et al. (2012)) is

$$\pi_{\text{curv}}(\boldsymbol{\theta}) \sim \mathbf{N}(\boldsymbol{\theta}_0, |\mathbf{n}|^{-1}\mathbf{G}^{-1}(\boldsymbol{\theta}_0)).$$

As shown in Guillaumin et al. (2022), the variance of the sampling distribution of the maximum spatial debiased Whittle likelihood estimator (MdWLE) $\hat{\boldsymbol{\theta}}_{\text{dW}}$ is

$$\text{Var}_{\boldsymbol{\theta}}[\hat{\boldsymbol{\theta}}_{\text{dW}}] \approx \mathbf{G}^{-1}(\boldsymbol{\theta}), \quad (18)$$

which has the same sandwich structure as the covariance of the MCLE in (16). Guillaumin et al. (2022) give an analytical form of the asymptotic distribution of the MdWLE for Gaussian

random fields when the observation domain \mathbf{n} grows to infinity in all directions; however, this form is seldom reached in practice. Simons and Olhede (2013) give a practical large-sample case where the asymptotic form has not been reached. In addition, empirical findings via simulations and, in the case of missing data, prevent the use of the exact form of the asymptotic variance for posterior adjustments. We therefore propose two methods that estimate the adjustment quantities via simulation.

3.3 Two curvature adjustments

This section explains the computation of the sandwich matrix in (18) and proposes two ways of computing the corresponding adjustment matrix \mathbf{C} specific to the debiased spatial Whittle likelihood. The computation of the analytic form of (18) is intractable for larger grids for the reasons explained below, and thus, we resort to Monte Carlo simulation when computing the adjustment matrix \mathbf{C} . The computation of the adjustment matrices is performed once before the MCMC simulation at a one-time cost.

Guillaumin et al. (2022) give an analytic form \mathbf{H} of the Fisher information matrix

$$\mathbf{H}(\boldsymbol{\theta}) = \frac{1}{2} \sum_{\boldsymbol{\omega} \in \Omega_{\mathbf{n}_k}} \bar{I}_{\mathbf{n}_k}(\boldsymbol{\omega}; \boldsymbol{\theta})^{-2} \nabla_{\boldsymbol{\theta}} \bar{I}_{\mathbf{n}_k}(\boldsymbol{\omega}; \boldsymbol{\theta}) \nabla_{\boldsymbol{\theta}} \bar{I}_{\mathbf{n}_k}(\boldsymbol{\omega}; \boldsymbol{\theta})^{\top},$$

where $\nabla_{\boldsymbol{\theta}} \bar{I}_{\mathbf{n}}(\boldsymbol{\omega}; \boldsymbol{\theta})$ is the gradient of the expected periodogram. This gradient can be computed efficiently via the FFT and using the same procedure as the expected periodogram, replacing the covariance function with its gradient; see Equation (38) in Guillaumin et al. (2022) for more details.

The i, j th element in the variance of the score vector, i.e. $\text{Var}_{\boldsymbol{\theta}}[\nabla_{\boldsymbol{\theta}} \ell_{\text{dW}}(\boldsymbol{\theta})]$, is given as

$$\text{cov} \left[\frac{\partial \ell_{\text{dW}}(\boldsymbol{\theta})}{\partial \theta_i}, \frac{\partial \ell_{\text{dW}}(\boldsymbol{\theta})}{\partial \theta_j} \right] = |\mathbf{n}|^{-2} \sum_{\boldsymbol{\omega}_1, \boldsymbol{\omega}_2 \in \Omega_{\mathbf{n}}} \frac{\text{cov}[I_{\mathbf{n}}(\boldsymbol{\omega}_1), I_{\mathbf{n}}(\boldsymbol{\omega}_2)]}{\bar{I}_{\mathbf{n}}^2(\boldsymbol{\omega}_1; \boldsymbol{\theta}), \bar{I}_{\mathbf{n}}^2(\boldsymbol{\omega}_2; \boldsymbol{\theta})} \frac{\partial \bar{I}_{\mathbf{n}}(\boldsymbol{\omega}_1; \boldsymbol{\theta})}{\partial \theta_i} \frac{\partial \bar{I}_{\mathbf{n}}(\boldsymbol{\omega}_2; \boldsymbol{\theta})}{\partial \theta_j}.$$

This exact form involves a summation over $|\mathbf{n}|^2$ terms, with each term itself requiring the evaluation of the covariance of the periodogram at two Fourier frequencies. Thus, a naive implementation would require $\mathcal{O}(|\mathbf{n}|^3)$ elementary operations in the case of a Gaussian random field, and might prove even more challenging without the assumption of Gaussianity. Making use of the fast Fourier transform, the computational cost may be brought down to $\mathcal{O}(|\mathbf{n}|^2 \log |\mathbf{n}|)$ for a Gaussian random field, but this remains intractable even for moderate grid sizes. Our adjustments that we now turn to circumvent these computational issues by approximating the variance of the score.

Our first adjustment is based on the Monte Carlo estimate of $\text{Var}_{\boldsymbol{\theta}}[\nabla_{\boldsymbol{\theta}} \ell_{\text{dW}}(\boldsymbol{\theta})]$,

$$\mathbf{J}(\boldsymbol{\theta}) \approx \hat{\mathbf{J}}(\boldsymbol{\theta}) = \frac{1}{M-1} \sum_{i=1}^M \left(\mathbf{g}^{(i)} - \bar{\mathbf{g}} \right) \left(\mathbf{g}^{(i)} - \bar{\mathbf{g}} \right)^{\top}, \quad (19)$$

where $\mathbf{g}^{(i)} = \nabla_{\boldsymbol{\theta}} \ell_{\text{dW}}(\widehat{\boldsymbol{\theta}}_{\text{dW}} | X_{\mathbf{s}}^{(i)})$ and $\bar{\mathbf{g}}$ denotes the sample mean of the estimates. Once the MdWLE given the observed data is found, we simulate M random fields from the specified model conditional on $\widehat{\boldsymbol{\theta}}_{\text{dW}}$. Then, $\widehat{\mathbf{J}}(\boldsymbol{\theta})$ is obtained as the empirical covariance estimator based on M Monte Carlo samples of the gradient $\nabla_{\boldsymbol{\theta}} \ell_{\text{dW}}(\widehat{\boldsymbol{\theta}}_{\text{dW}} | X_{\mathbf{s}}^{(i)})$. Note that simulation of Gaussian random fields can be performed efficiently in $\mathcal{O}(|\mathbf{n}| \log |\mathbf{n}|)$ time via circulant embedding (Dietrich and Newsam, 1997). The adjustment is obtained as

$$\mathbf{C}_1 = \mathbf{M}^{-1} \widetilde{\mathbf{M}}_A, \quad (20)$$

$$\widetilde{\mathbf{M}}_A^\top \widetilde{\mathbf{M}}_A = \mathbf{H}(\boldsymbol{\theta}_0) \widehat{\mathbf{J}}(\boldsymbol{\theta}_0)^{-1} \mathbf{H}(\boldsymbol{\theta}_0), \quad \mathbf{M}^\top \mathbf{M} = \mathbf{H}(\boldsymbol{\theta}_0), \quad (21)$$

where $\widetilde{\mathbf{M}}_A^\top \widetilde{\mathbf{M}}_A$ and $\mathbf{M}^\top \mathbf{M}$ are singular value decompositions of their respective matrices. Note that $\widetilde{\mathbf{M}}_A$ is an estimate of \mathbf{M}_A , however, since (19) converges in probability to $\mathbf{J}(\boldsymbol{\theta})$ (weak law of large numbers) it follows that $\mathbf{H}(\boldsymbol{\theta}_0) \widehat{\mathbf{J}}(\boldsymbol{\theta}_0)^{-1} \mathbf{H}(\boldsymbol{\theta}_0)$ in (21) converges in probability to $\mathbf{G}(\boldsymbol{\theta}_0)$ by the continuous mapping theorem (provided $\mathbf{J}(\boldsymbol{\theta}_0)$ is invertible). Thus $\widetilde{\mathbf{M}}_A$ also converges in probability to \mathbf{M}_A .

The second adjustment has two key features. First, it directly estimates the sandwich matrix by a Monte Carlo estimate of $\text{Var}_{\boldsymbol{\theta}}[\widehat{\boldsymbol{\theta}}_{\text{dW}}]$,

$$\text{Var}_{\boldsymbol{\theta}}[\widehat{\boldsymbol{\theta}}_{\text{dW}}] \approx \widehat{\mathbf{G}^{-1}(\widehat{\boldsymbol{\theta}}_{\text{dW}})} = \frac{1}{M-1} \sum_{i=1}^M \left(\widetilde{\boldsymbol{\theta}}_{\text{dW}}^{(i)} - \overline{\widetilde{\boldsymbol{\theta}}_{\text{dW}}} \right) \left(\widetilde{\boldsymbol{\theta}}_{\text{dW}}^{(i)} - \overline{\widetilde{\boldsymbol{\theta}}_{\text{dW}}} \right)^\top, \quad (22)$$

where $\widetilde{\boldsymbol{\theta}}_{\text{dW}}^{(i)}$, for $i = 1, \dots, M$ are the MdWLE from M datasets simulated at $\widehat{\boldsymbol{\theta}}_{\text{dW}}$. Simulating data $X_{\mathbf{s}}^{(i)}$ from the likelihood at $\widehat{\boldsymbol{\theta}}_{\text{dW}}$ and finding the corresponding MdWLE for M iterations gives the simulation approximation of the MdWLE distribution. Second, the observed Fisher information matrix, which we denote $\mathcal{H}(\boldsymbol{\theta})$, of $\ell_{\text{dW}}(\boldsymbol{\theta})$ is used in place of $\mathbf{H}(\boldsymbol{\theta})$ when computing \mathbf{M} . The observed Fisher information is an unbiased estimator of the Fisher information, which matches the curvature of the unadjusted debiased Whittle likelihood, providing a tailored curvature adjustment for the specific dataset. Hence, the adjustment is

$$\mathbf{C}_2 = \widehat{\mathbf{M}}^{-1} \widetilde{\mathbf{M}}_A, \quad (23)$$

$$\widetilde{\mathbf{M}}_A^\top \widetilde{\mathbf{M}}_A = \widehat{\mathbf{G}}(\boldsymbol{\theta}), \quad \widehat{\mathbf{M}}^\top \widehat{\mathbf{M}} = \mathcal{H}(\boldsymbol{\theta}), \quad (24)$$

where $\widetilde{\mathbf{M}}_A^\top \widetilde{\mathbf{M}}_A$ and $\widehat{\mathbf{M}}^\top \widehat{\mathbf{M}}$ are singular value decompositions of their respective matrices.

We denote the curvature-adjusted debiased Whittle likelihoods as

$$\ell_{\text{dW}}^{(i)}(\boldsymbol{\theta}) = \ell_{\text{dW}}(\boldsymbol{\theta}^*), \quad \boldsymbol{\theta}^* = \widehat{\boldsymbol{\theta}}_{\text{dW}} + \mathbf{C}_i(\boldsymbol{\theta} - \widehat{\boldsymbol{\theta}}_{\text{dW}}), \quad \text{for } i = 1, 2. \quad (25)$$

Combining $\ell_{\text{dW}}^{(i)}(\boldsymbol{\theta})$ with a specified prior $p(\boldsymbol{\theta})$ in a Metropolis-Hastings algorithm targets the desired posterior density $\pi_{\text{dW}}^{(i)}(\boldsymbol{\theta})$ for $i = 1, 2$. Algorithms 1 and 2 describe the computations necessary to obtain adjustments \mathbf{C}_1 and \mathbf{C}_2 , respectively.

3.4 Recommendations

We now discuss some important considerations and recommendations for both curvature adjustments. The \mathbf{C}_1 matrix requires the evaluation of $\nabla_{\boldsymbol{\theta}} \ell_{\text{dW}}(\boldsymbol{\theta})$, which requires the gradient of the covariance function wrt the parameters. It is well known that the gradient of the Matérn kernel in (1) wrt ν exists analytically but is difficult and computationally expensive. For this reason, we restrict the use of \mathbf{C}_1 for fixed ν ; however, it is possible to apply approaches such as Geoga et al. (2023) for the Matérn kernel.

Both adjustments employ Monte Carlo estimation. The variance of the Monte Carlo estimates is an important consideration when choosing M to compute the adjustments. Thus, for cases when the variance is higher, a larger M is required. Generally, small and moderate grid sizes require larger M , e.g. $M = 1000$.

The \mathbf{C}_1 adjustment performs a Monte Carlo estimate of $\text{Var}_{\boldsymbol{\theta}} [\nabla_{\boldsymbol{\theta}} \ell_{\text{dW}}(\boldsymbol{\theta})]$, whereas the \mathbf{C}_2 adjustment estimates $\text{Var}_{\boldsymbol{\theta}} [\hat{\boldsymbol{\theta}}_{\text{dW}}]$. We have observed that the variance of $\text{Var}_{\boldsymbol{\theta}} [\hat{\boldsymbol{\theta}}_{\text{dW}}]$ is large when the domain size is small relative to the value of ρ . In this case, we recommend using \mathbf{C}_1 since $\text{Var}_{\boldsymbol{\theta}} [\nabla_{\boldsymbol{\theta}} \ell_{\text{dW}}(\boldsymbol{\theta})]$, and the variance thereof is less sensitive to ρ compared to the domain size. However, for more difficult settings such as missing data and irregular domains, the estimate of $\text{Var}_{\boldsymbol{\theta}} [\hat{\boldsymbol{\theta}}_{\text{dW}}]$ may be a better approximation of $\mathbf{G}^{-1}(\boldsymbol{\theta})$ (or its inverse) compared to the \mathbf{C}_1 adjustment. Additionally, the computation of $\nabla_{\boldsymbol{\theta}} \ell_{\text{dW}}(\boldsymbol{\theta})$ for \mathbf{C}_1 may not be known in closed form for missing data and/or irregular domains. Note that while the adjustment based on \mathbf{C}_2 may be more accurate, it is also computationally more burdensome, particularly for larger grids, due to the optimization of the likelihood for each $\hat{\boldsymbol{\theta}}_{\text{dW}}^{(i)}$ in (22) which can require multiple evaluations of $\ell_{\text{dW}}(\boldsymbol{\theta})$.

Another important phenomenon is when the adjusted likelihood becomes flat. If elements of \mathbf{C} , particularly on the diagonal, are small, the vector $\mathbf{C}(\boldsymbol{\theta} - \hat{\boldsymbol{\theta}}_{\text{dW}})$ in (25), becomes small. Thus for a proposed $\boldsymbol{\theta}$ that is far from $\hat{\boldsymbol{\theta}}_{\text{dW}}$, the adjusted parameter $\boldsymbol{\theta}^*$ will still be close to $\hat{\boldsymbol{\theta}}_{\text{dW}}$. As a consequence, the adjusted likelihood becomes flat around $\hat{\boldsymbol{\theta}}_{\text{dW}}$, and the corresponding posterior will be dominated by the prior. To minimize the influence of the prior on the adjusted likelihood, a non-informative prior such as the penalised complexity (PC) prior is recommended, described in more detail in Section 3.

Algorithm 1 Adjustment C_1 .

Input: MdWLE $\hat{\theta}_{\text{dW}}$

- 1: **for** $i = 1, \dots, M$ **do in parallel**
- 2: Simulate $X_s^{(i)} \sim p(X_s | \hat{\theta}_{\text{dW}})$.
- 3: Compute $\nabla_{\theta} \ell_{\text{dW}}(\hat{\theta}_{\text{dW}} | X_s^{(i)})$.
- 4: **end for**
- 5: Compute $\hat{J}(\hat{\theta}_{\text{dW}})$ from (19).

6: Factor

$$\begin{aligned} M^{\top} M &= H(\hat{\theta}_{\text{dW}}) \\ \widetilde{M}_A^{\top} \widetilde{M}_A &= H(\hat{\theta}_{\text{dW}}) \hat{J}(\hat{\theta}_{\text{dW}})^{-1} H(\hat{\theta}_{\text{dW}}). \end{aligned}$$

7: **Return** $C_1 = M^{-1} \widetilde{M}_A$.

Algorithm 2 Adjustment C_2

Input: MdWLE $\hat{\theta}_{\text{dW}}$.

- 1: **for** $i = 1, \dots, M$ **do in parallel**
- 2: Simulate $X_s^{(i)} \sim p(X_s | \hat{\theta}_{\text{dW}})$.
- 3: $\widetilde{\theta}_{\text{dW}}^{(i)} = \arg \min_{\theta \in \Theta} \ell_{\text{dW}}(\theta | X_s^{(i)})$.
- 4: **end for**
- 5: Compute $\text{Var}_{\theta} [\hat{\theta}_{\text{dW}}] \approx \widehat{G^{-1}(\hat{\theta}_{\text{dW}})}$ from (22).

6: Factor

$$\begin{aligned} \widehat{M}^{\top} \widehat{M} &= \mathcal{H}(\hat{\theta}_{\text{dW}}) \\ \widetilde{M}_A^{\top} \widetilde{M}_A &= \widehat{G}(\hat{\theta}_{\text{dW}}). \end{aligned}$$

7: **Return** $C_2 = \widehat{M}^{-1} \widetilde{M}_A$.

Table 1: Algorithms for the adjustments C_1 (Algorithm 1) and C_2 (Algorithm 2).

3.5 Simulation study

We use the computational approach of Monahan and Boos (1992) to validate the coverages of the curvature adjustments in Section 3. This approach was later formalized into a software validation algorithm in Cook et al. (2006). First, simulate $i = 1, \dots, K$ independent samples from the prior, $\theta^{(i)} \sim p(\theta)$, and for each $\theta^{(i)}$, generate a random field $X_s^{(i)} \sim p(X_s | \theta^{(i)})$ and compute the integral

$$U^{(i)} = \int_{-\infty}^{\theta^{(i)}} \widetilde{p}(\theta | X_s^{(i)}) d\theta, \quad \text{for } i = 1, \dots, K, \quad (26)$$

where $\widetilde{p}(\theta | X_s^{(i)})$ is a quasi-posterior. A Monte Carlo estimate $\widehat{U}^{(i)}$ of the above integral is performed with M samples from the quasi-posterior via the random walk Metropolis-Hasting algorithm. Cook et al. (2006) proves that if $\widetilde{p}(\theta | X_s^{(i)}) = p(\theta | X_s^{(i)})$ then $\widehat{U}^{(i)} \xrightarrow{d} \text{Unif}(0, 1)$ as $M \rightarrow \infty$, for each $i = 1, \dots, K$. Hence, a QQ-plot of the $\widehat{U}^{(i)}$ against the uniform distribution can be used to detect miscalibration of a quasi-posterior.

Since the two proposed curvature adjustments are valid asymptotically, we construct a simulation study to verify this for increasing grid sizes. We consider various priors and covariance kernels. The three Whittle likelihoods considered are:

1. $\ell_{\text{dW}}(\theta)$, the unadjusted debiased spatial Whittle likelihood.
2. $\ell_{\text{dW}}^{(1)}(\theta)$, the C_1 -adjusted debiased spatial Whittle likelihood.
3. $\ell_{\text{dW}}^{(2)}(\theta)$, the C_2 -adjusted debiased spatial Whittle likelihood.

For all simulations, $M = 250$ datasets are generated from a two-dimensional Gaussian random field with a Matérn covariance kernel.

Simulation 1. Consider a two-dimensional Gaussian random field from a Matérn covariance kernel with $\nu \rightarrow \infty$, known as the squared-exponential covariance kernel, defined as

$$c(\mathbf{u}|\rho, \sigma) = \sigma^2 \exp\left(-\frac{\|\mathbf{u}\|^2}{2\rho^2}\right).$$

The spectral density is $2\pi\rho \exp(-2\pi^2\rho^2\|\boldsymbol{\omega}\|^2)$ (Rasmussen and Williams, 2006). This produces overly smooth simulations due to high spectral mass at the lower frequencies, whereas the higher frequencies have a negligible mass. Estimation with this kernel is difficult since the periodogram contains significant correlations between Fourier frequencies. We use independent Gamma priors, $\rho \sim \text{Gamma}(\alpha = 60, \beta = 10)$, $\sigma \sim \text{Gamma}(\alpha = 60, \beta = 50)$, with means $E[\rho] = 6$ and $E[\sigma] = 1.2$, respectively. We also use square grids with no missing values and grid sizes $|\mathbf{n}| = (256^2, 512^2, 1024^2)$.

Figure 3 displays the QQ-plots of the standard uniform distribution against $\widehat{U}^{(i)}$ for $i = 1, \dots, K$ for each grid size and adjustment. The unadjusted debiased Whittle posterior (top row) yields quantiles that are far from uniform for all three grid sizes. The S-shape of the QQ-plots suggests that the unadjusted posteriors are heavily over-concentrated and therefore rarely cover the true parameter $\boldsymbol{\theta}_0$. The two adjusted posteriors, \mathbf{C}_1 in the middle row and the \mathbf{C}_2 adjustment in the bottom row, have dramatically better coverage properties than the unadjusted case. For the two larger grid sizes, the adjusted posteriors give almost perfectly calibrated posteriors.

Simulation 2. We consider an irregular domain shape for this simulation. The domain shape is a grid of France. The grid is of size $\mathbf{n} = (500, 500)$, and the 62% of the grid points outside the border of France are treated as missing values. We use a squared-exponential covariance kernel with independent gamma priors, $\rho \sim \text{Gamma}(\alpha = 120, \beta = 20)$, $\sigma \sim \text{Gamma}(\alpha = 50, \beta = 50)$, with means $E[\rho] = 6$ and $E[\sigma] = 1$. We simulate $M = 1000$ datasets to compute the \mathbf{C}_1 and \mathbf{C}_2 adjustments.

Figure 4 shows the QQ-plot of the posterior quantiles. As expected, the unadjusted debiased Whittle model fails to provide proper coverages for both parameters. The \mathbf{C}_1 and \mathbf{C}_2 adjustments are similar for both parameters, with \mathbf{C}_2 performing marginally better than \mathbf{C}_1 . Both adjustments are indistinguishable from a standard uniform between $(0, 0.5)$; however, the top half interval seems to have more concentration of mass compared to the bottom interval, with ρ performing slightly worse than σ .

Simulation 3. We consider the penalised complexity (PC) prior for random fields proposed in Fuglstad et al. (2019). The PC prior is for Matérn Gaussian random fields on the joint parameter space, range ρ and amplitude σ , for a fixed smoothness $\nu = \infty$ (squared-exponential kernel). This prior can provide physically meaningful interpretations via its selection of hyperparameters. Furthermore, it is weakly informative and shrinks the range parameter towards infinity and the amplitude parameter towards zero. For two-dimensional random fields with

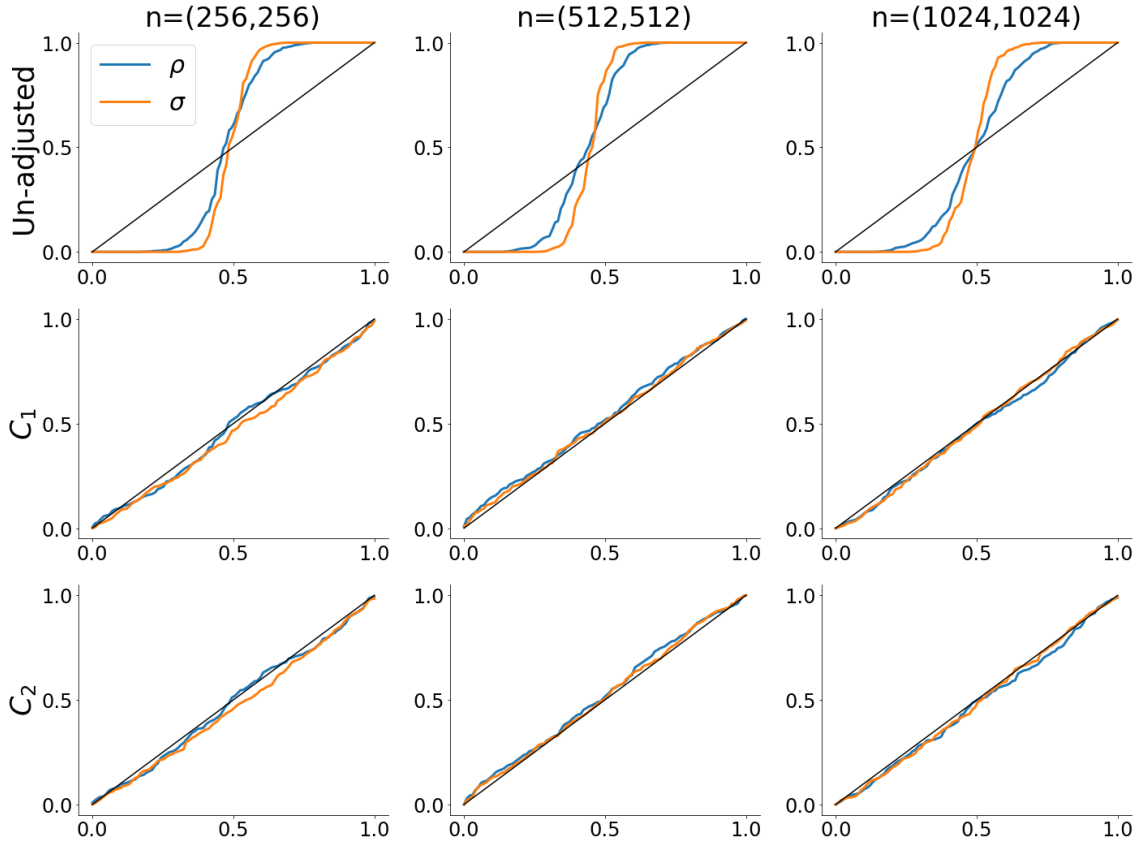


Figure 3: Simulation 1. Standard uniform QQ-plots to quantify the coverage of quasi-posteriors for kernel hyperparameters of the Gaussian random field.

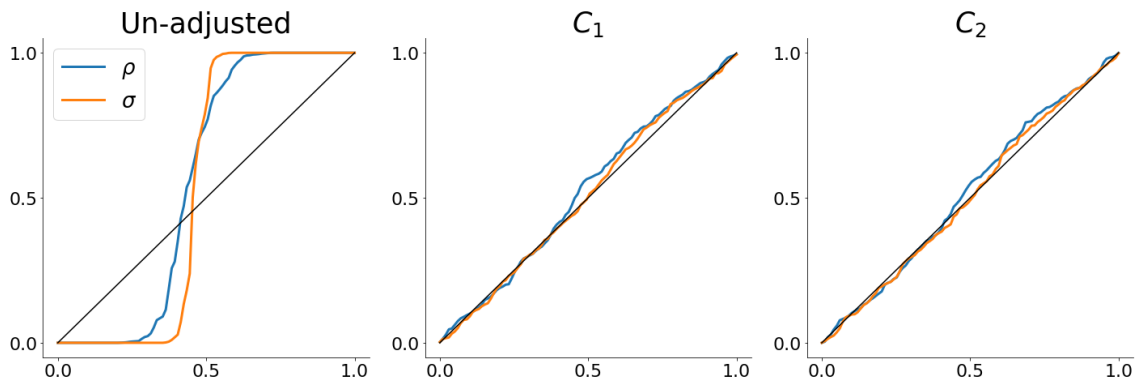


Figure 4: Simulation 2. Standard uniform QQ-plots to quantify the coverage of quasi-posteriors for kernel hyperparameters of the Gaussian random field for an irregular domain shape of France.

fixed ν , the density of the PC prior is given as

$$p(\rho, \sigma) = \lambda_1 \lambda_2 \rho^{-2} \exp(-\lambda_1 \rho^{-1} - \lambda_2 \sigma),$$

where $\rho, \sigma > 0$, and

$$\lambda_1 = -\log(\alpha_1)p_0, \quad \text{and} \quad \lambda_2 = -\frac{\log(\alpha_2)}{\sigma_0},$$

with hyperparameters $\Pr(\rho < \rho_0) = \alpha_1$ and $\Pr(\sigma > \sigma_0) = \alpha_2$. To obtain samples from the prior, we take log transformations, $\log(\rho)$ and $\log(\sigma)$, and perform MCMC on the transformed space. For the simulation settings, we select hyperparameters $(\rho_0, \sigma_0, \alpha_1, \alpha_2) = (0.7, 1.0, 0.05, 0.05)$. Similar to Simulation 1, we consider square grids with no missing values with grid sizes $|\mathbf{n}| = (256^2, 512^2, 1024^2)$.

Since the PC prior exhibits heavy tails for ρ , simulating data via circulant embedding and estimation is unfeasible when drawing large values of ρ relative to the domain size. Thus, the corresponding quantiles in (26) are set to one for large proposed values of ρ . Additionally, the corresponding quantiles are set to zero for amplitudes that are extremely close to zero.

Figure 5 displays the QQ-plots for the coverage with the PC prior. For $|\mathbf{n}| = 256^2$, the results for both \mathbf{C}_1 and \mathbf{C}_2 are close to uniform, whereas that of the unadjusted debiased Whittle posterior is not. All three posteriors are close to uniform for $|\mathbf{n}| = 512^2$, with both adjustments being almost indistinguishable from the standard uniform. In the case of $|\mathbf{n}| = 1024^2$, the \mathbf{C}_1 and \mathbf{C}_2 adjustments are very close to uniform, whereas the unadjusted is slightly worse for the ρ parameter. Surprisingly, all posteriors for the σ parameter are slightly worse for the largest grid size compared to the smaller grid sizes; note, however, that the posterior is naturally more concentrated for the largest grid size, so a slightly miscalibrated posterior variance can have a large effect.

4 Applications

We illustrate our method on two popular datasets in the literature and compare our approach to the standard Whittle likelihood and the unadjusted debiased Whittle likelihood. The first example, sea surface temperature, is suited for the \mathbf{C}_2 adjustment since we assumed a Matérn covariance kernel and also estimate the slope parameter ν . As mentioned previously, the gradients of the Matérn kernel wrt the parameters are difficult to compute, thus disqualifying \mathbf{C}_1 . The second example, photosynthetically active radiation data, however, is suited for both adjustments. For a more detailed discussion of the suitability of each adjustment, refer to Section 3.4.

4.1 Sea surface temperature

The first application is tropical rainfall measuring mission (TRMM) microwave imager (TMI) satellite data from the Pacific Ocean presented in Chapter 5 of Gelfand et al. (2010). Sea

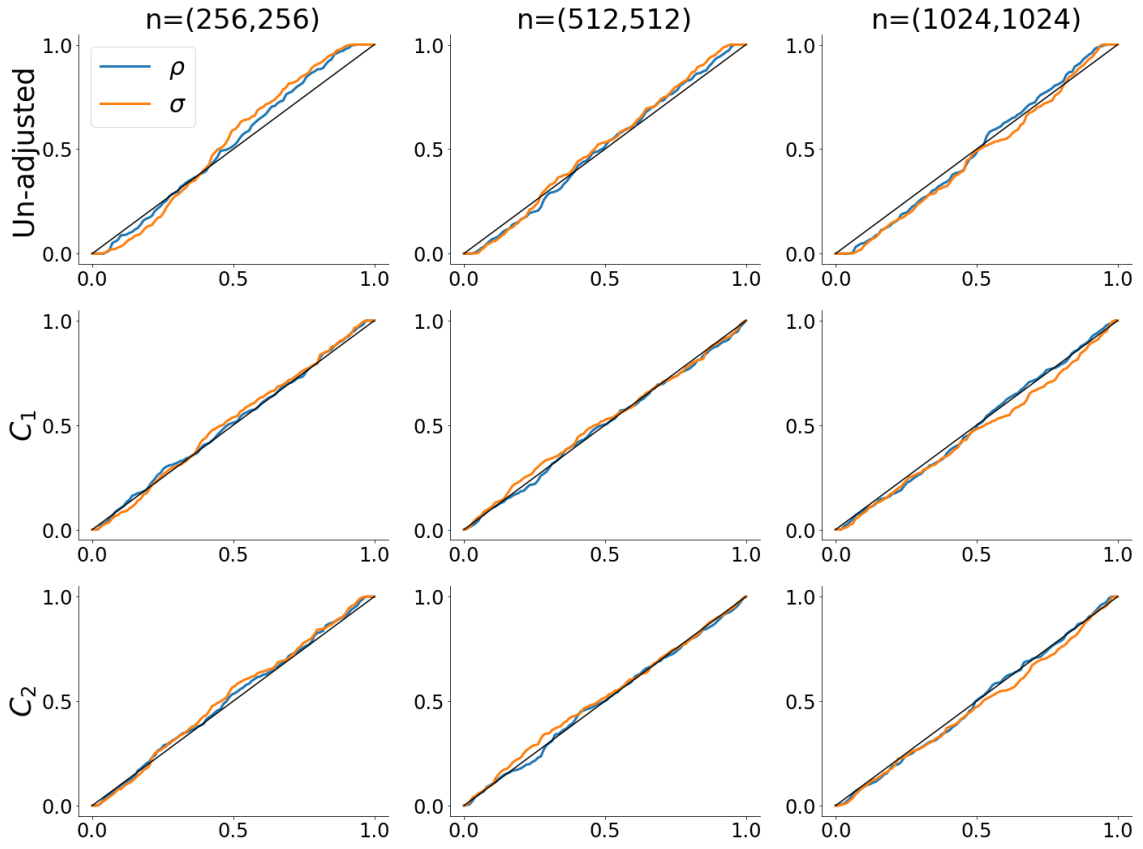


Figure 5: Simulation 3. Standard uniform QQ-plots to quantify the coverage of quasi-posteriors for kernel hyperparameters of the Gaussian random field with the PC prior.

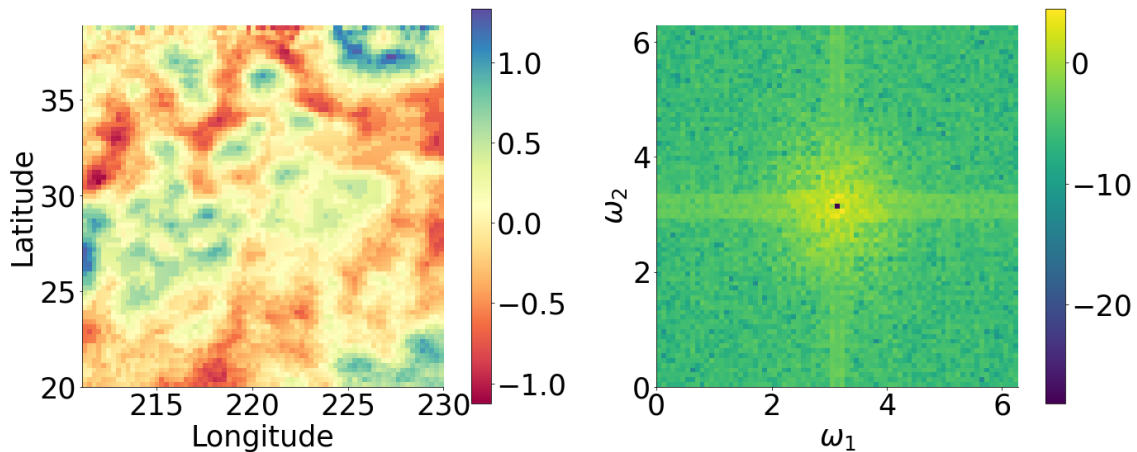


Figure 6: Sea surface temperatures over the Pacific Ocean. The left plots show the processed data after removing the trend. The right plot is the un-tapered log-periodogram of the data.

surface temperature (SST) data are used for climate modelling and meteorology and are essential for evaluating climate change. They are also helpful for comparison with oceanic climate models as a diagnostic tool. Identifying spatial patterns of SST is a critical factor in the formation of hurricanes in the Pacific Ocean, which strike Central America. Furthermore, the transfer of water between the northern and southern equatorial currents is an important application of the analysis of the spatial structure of SST. Quantifying spatial variability and making informed predictions about SST is crucial for research on the world's ocean and the broader climate. The data are available at https://images.remss.com/tmi/tmi_data_daily.html.

The SST data, in degrees Celsius, is from March 1998 and has roughly a $25\text{km} \times 25\text{km}$ spatial resolution defined by latitude and longitude. The data are observed on a rectangular grid of size 75×75 . Due to the large number of observations, maximum likelihood estimation, let alone Bayesian inference via the Gaussian likelihood, is computationally expensive. Instead, we use the proposed Bayesian inference method using frequency domain methods.

To satisfy the stationarity assumption, Gelfand et al. (2010) suggest removing a second-order polynomial mean trend

$$\beta_0 + \beta_1 u(\mathbf{s}) + \beta_2 v(\mathbf{s}) + \beta_3 u(\mathbf{s})^2 + \beta_4 v(\mathbf{s})^2 + \beta_5 u(\mathbf{s})v(\mathbf{s}),$$

where $u(\mathbf{s})$ and $v(\mathbf{s})$ are the longitude and latitude at each observation respectively. Figure 6 displays the stationary random field and its corresponding log-periodogram.

We also follow the suggestions from Gelfand et al. (2010) and use the Matérn covariance kernel in (1) as an appropriate model. Initial optimisations are performed to obtain a sensible fixed value for the nugget parameter $\sigma_\varepsilon^2 = 10^{-10}$. We perform Bayesian inference over the joint parameter space $\boldsymbol{\theta} = (\rho, \sigma, \nu)$. This is a challenging problem as it is well known that the smoothness parameter ν is difficult to estimate due to the lack of information in the likelihood

(De Oliveira and Han, 2022).

We compare three posteriors: the unadjusted Debiased Whittle, the adjusted Debiased Whittle with \mathbf{C}_2 and the standard Whittle. Note that the \mathbf{C}_1 adjustment cannot be applied here as this requires the derivatives of the Matérn covariance wrt the parameters, which do not always exist. We simulate $M = 500$ datasets to compute the adjustment \mathbf{C}_1 matrix. Independent Gamma priors are used for all three parameters,

$$\rho \sim \text{Gamma}(\alpha = 5, \beta = 1.0), \quad \sigma \sim \text{Gamma}(\alpha = 0.7, \beta = 1/0.7), \quad \nu \sim \text{Gamma}(\alpha = 1.0, \beta = 2).$$

Figure 7 plots the marginal posteriors from the different methods. The figure shows that the standard Whittle gives lower estimates of the ρ and σ than the debiased Whittle. The \mathbf{C}_2 adjustment in orange inflates the variance compared to the unadjusted debiased Whittle in blue. Overall, we conclude that the adjustment significantly reshapes the posterior. With support from the simulation studies in Section 3.5, this demonstrates the importance of the posterior adjustments in avoiding misleading inferences also on real data.

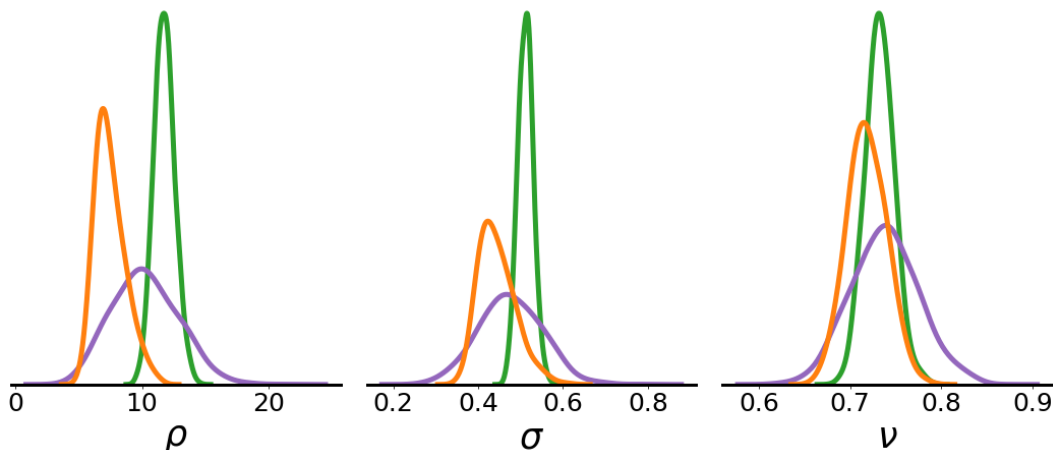


Figure 7: Sea surface temperatures: Kernel density estimates of the marginal posteriors of the kernel hyperparameters. The standard Whittle in orange, the unadjusted debiased Whittle in green, and the \mathbf{C}_2 -adjusted debiased Whittle in purple.

To check the adequacy of the model, we use the parametric model of (11), and that if $X \sim \text{Exp}(\mu)$ then $U = 1 - \exp(-X/\mu) \sim \text{Unif}(0, 1)$, to define the frequency domain residual spectrum as

$$r_{\mathbf{n}}(\omega) = 1 - \exp(-I_{\mathbf{n}}(\omega) / \bar{I}_{\mathbf{n}}(\omega; \theta)) \stackrel{\text{i.i.d.}}{\sim} \text{Unif}(0, 1), \quad \omega \in \Omega_{\mathbf{n}},$$

for the \mathbf{C}_2 -adjusted debiased Whittle likelihood. Similarly, the residuals of the standard Whittle are obtained by replacing the expected periodogram with the spectral density. Ideally, given the correct model, the residuals have a standard uniform distribution throughout the entire observable domain. Figure 8 plots the standard Whittle residuals in the middle graph

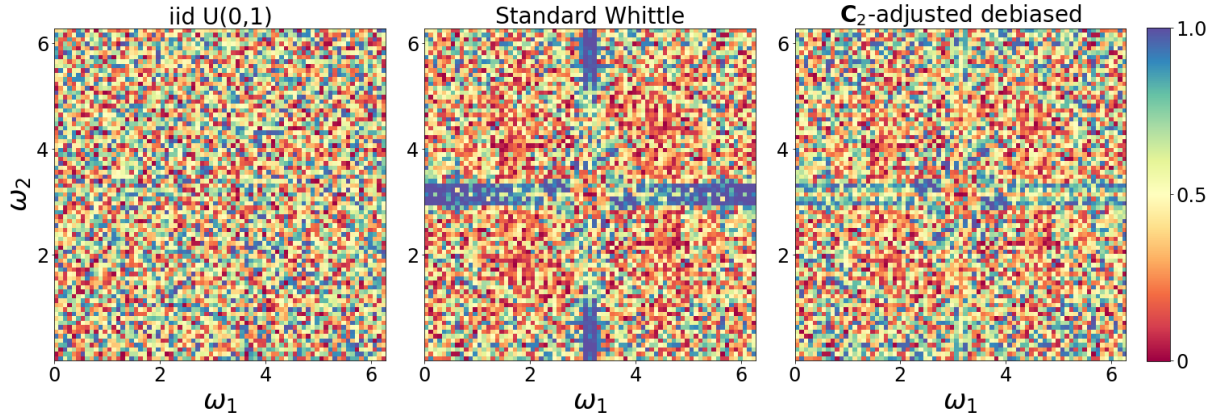


Figure 8: Residual spectrum $r_{\mathbf{n}}(\boldsymbol{\omega})$ in (4.1). The left plot is the idealized iid standard uniform, the middle plot is the standard Whittle, and the right plot is \mathbf{C}_2 adjusted debiased Whittle. The estimated spectra are based on the posterior mean.

and the \mathbf{C}_2 -adjusted debiased Whittle on the right using their associated posterior means; a simulation of the ideal case with a perfectly fitting model is shown on the leftmost graph as a reference. The residual spectrum in the middle graph from the standard Whittle model have very large and clearly visible side lobes, suggesting a poorly fitting model. The residual spectrum from the \mathbf{C}_2 -adjusted debiased Whittle in the right hand graph has a little excess side lobes in the horizontal direction, but is overall quite close to the ideal iid Unif(0, 1) case.

4.2 Photosynthetically active radiation data

We consider the NASA satellite data analysed in Guinness and Fuentes (2017). Photosynthetically active radiation (PAR) data contain the spectral range (in the interval 400-700 nanometers) of solar radiation used in photosynthesis. PAR is an integral part of primary producers such as phytoplankton, seagrass, plant growth, and species interaction. A deficiency of PAR can result in reduced growth or loss of corals, seagrass, and other photosynthetic organisms. Thus, PAR measurements give crucial insight into the quality and quantity of biological ecosystems. This dataset is from December 1, 2013, and can be found at <https://oceandata.sci.gsfc.nasa.gov/l3/>.

The data are located over the coast of Mexico, in Baja, California, with an evenly spaced grid size of 120 longitude values and 100 latitude values with an approximate resolution of $1/12^\circ$ for both longitude and latitude. The data have a total number of lattice locations of 12000. However, there are a total of 2270 missing values in the dataset for two reasons. First, PAR is measured over water, and thus, there are no readings over the land area. Second, the data are missing due to cloud cover. Our aim is to simulate the posterior of the parameters of the covariance kernel by applying the methods we developed and give some meaningful predictions of the missing observations due to cloud cover. The data are plotted in Figure 9. The large black triangular region contains missing values due to cloud cover, whereas the

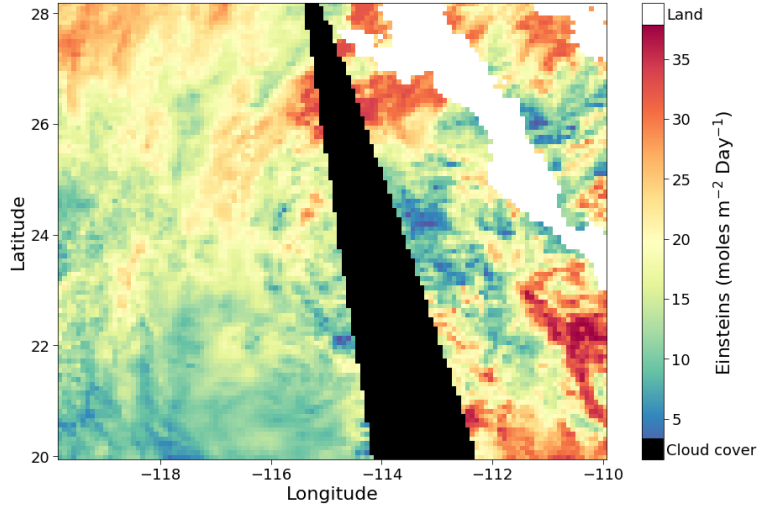


Figure 9: Photosynthetically active radiation (PAR) data over the coast of Mexico in Baja California. The Black pixels represent missing data due to cloud cover, whereas the white pixels are missing data due to land.

white values are missing due to land.

We follow Guinness and Fuentes (2017) and subtract the empirical mean of the data since there are no apparent trends in the data. Furthermore, we use an exponential covariance kernel with unknown parameters $\theta = (\rho, \sigma)$. As in the previous example, initial optimizations are performed to obtain a sensible fixed value for the nugget parameter $\sigma_\epsilon^2 = 0.001$. We compare four methods: the standard Whittle likelihood, the un-adjusted debiased spatial Whittle likelihood, the \mathbf{C}_1 -adjusted debiased spatial Whittle likelihood and the \mathbf{C}_2 -adjusted debiased spatial Whittle likelihood. The parameters of interest θ were transformed to the log-scale, and the PC prior was used for all methods with hyperparameter setting $(\rho_0, \sigma_0, \alpha_1, \alpha_2) = (0.7, 1.0, 0.05, 0.05)$, which is the same as in the simulation study.

The kernel density estimates of the marginal posteriors are plotted in Figure 10. The standard Whittle posteriors have lower estimates for ρ and σ on average than its debiased Whittle counterparts. Furthermore, while the debiased Whittle posteriors correct for the bias of the Whittle likelihood, its posteriors are most likely too concentrated, judging from the simulation results in Section 3.5. The \mathbf{C}_1 and \mathbf{C}_2 adjusted debiased Whittle posteriors in red and purple, respectively, produce very similar marginal posteriors and have larger variances than the unadjusted debiased Whittle.

Interpolation over missing values of the PAR data provides insight into the uncertainty over the missing regions while still accounting for the covariance properties of the data. Similar to Guinness and Fuentes (2017), Figure 11 shows three draws from the posterior predictive density, which is the conditional normal density

$$p(\tilde{X}(s_{cc})|X(s), \theta^{(i)}),$$

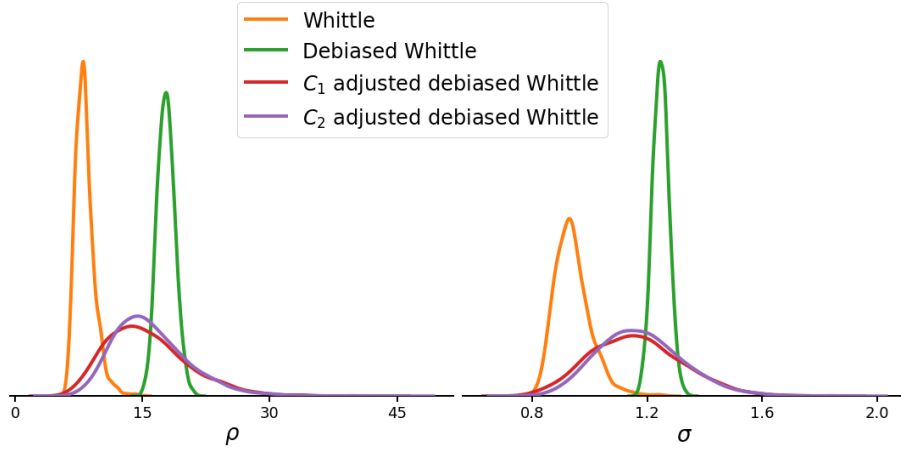


Figure 10: Kernel density estimates of the marginal posteriors for the photosynthetically active radiation data.

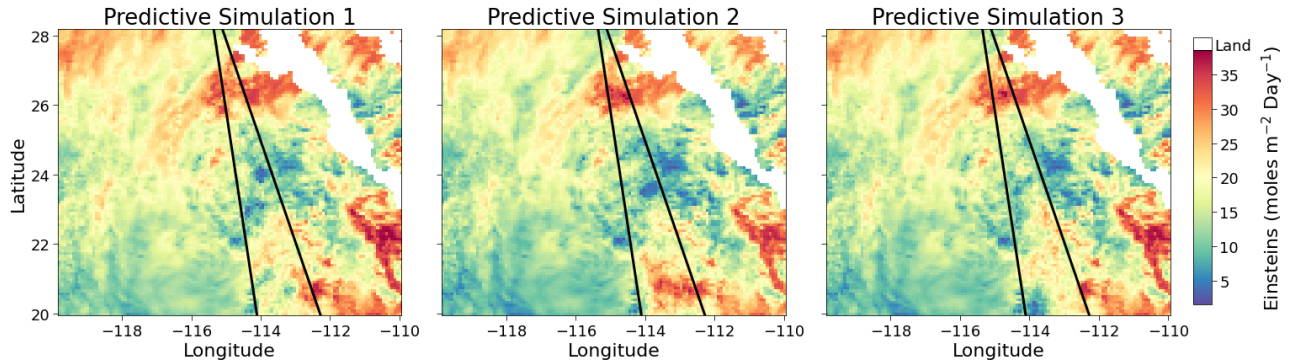


Figure 11: Three draws from the posterior predictive density with an exponential covariance model based on parameters from the MCMC chain at the 3000th (left), 6000th (middle), and 9000th (right) iteration.

where $i = 3000, 6000, 9000$ are the i th iterate of the MCMC chain based on the \mathbf{C}_1 -adjusted debiased Whittle, and \mathbf{s}_{cc} are the spatial locations of the missing data (triangular region indicated by the black lines) due to cloudcover.

5 Conclusion and future research

We propose a method to carry out Bayesian inference for covariance-stationary random fields using the computationally efficient debiased spatial Whittle likelihood recently proposed in the literature. In the classical paradigm, the debiased Whittle likelihood has many benefits discussed in Guillaumin et al. (2022) as opposed to other estimation methods (e.g. Whittle, 1954, Gelfand et al., 2010). However, because it is not a proper likelihood, its applicability to Bayesian inference needs careful treatment. Leveraging the fact that the debiased spatial Whittle likelihood falls within the framework of a pseudo-likelihood in finite samples, we use ideas from Ribatet et al. (2012) to construct posterior curvature adjustments that asymptot-

ically satisfy the Bernstein Von-Mises theorem for the subsequent adjusted debiased Whittle likelihood. These adjustments are designed to achieve appropriate coverage properties of the Bayesian posterior. The quantities needed to compute the posterior adjustments are not computationally tractable for the debiased spatial Whittle likelihood and we propose two methods to circumvent this. The first method works by computing the variance of the score function and is more robust to processes with large length scales. However, this adjustment relies on the derivative of the covariance function, which may not be analytically available for general Matérn class covariance functions. The second method estimates the adjustment via a simulation approximation of the sampling distribution of the MdWLE and the observed Fisher information, which provides a tailored adjustment useful in problems with smaller grid sizes. We demonstrate that both adjustments dramatically improve the coverages of the approximate posterior in simulated examples.

We see at least five directions for future research. First, one particular strength of our method is that it does not require the data to be Gaussian, and can therefore be extended to non-Gaussian spatial models. Second, for ultra-large spatial data, spectral subsampling MCMC (Salomone et al., 2020; Villani et al., 2024) is an attractive alternative if the log-likelihood function can be computed independently for each data point. As it stands, this is not possible/inefficient for the debiased Whittle likelihood since the expected periodogram is computed on the whole grid of Fourier frequencies via the FFT, or in the frequency domain by a convolution that requires the whole spectrum, so some innovation is needed to make this practical. An alternative is to use some other type of bias correction of the standard Whittle likelihood in a subsampling context, combined with the coverage adjustments used in this paper. Third, our proposed approach handles missing data and irregular domains, but more work is needed to extend it to irregularly spaced data (Matsuda and Yajima, 2009). Furthermore, although not explored here, our method can also be applied to time series models, i.e., when $d = 1$ (Sykulski et al., 2019), and is thus a useful alternative to the standard Whittle estimator for time series data with a small number of observations. Finally, other methods of calibration can be explored. For example, the recent approach in Frazier et al. (2023).

References

- Akaike, H. (1973). Block Toeplitz matrix inversion. *SIAM Journal on Applied Mathematics*, 24(2):234–241.
- Anitescu, M., Chen, J., and Stein, M. L. (2017). An inversion-free estimating equations approach for Gaussian process models. *Journal of Computational and Graphical Statistics*, 26(1):98–107.
- Berliner, L. M., Wikle, C. K., and Cressie, N. (2000). Long-lead prediction of Pacific SSTs via Bayesian dynamic modeling. *Journal of Climate*, 13(22):3953–3968.
- Best, N. G., Ickstadt, K., Wolpert, R. L., and Briggs, D. J. (2001). Combining models of health and exposure data: the SAVIAH study. In *Spatial Epidemiology: Methods and Applications*. Oxford University Press.
- Bevilacqua, M. and Gaetan, C. (2015). Comparing composite likelihood methods based on pairs for spatial Gaussian random fields. *Statistics and Computing*, 25:877–892.
- Brockwell, P. J. and Davis, R. A. (2009). *Time Series: Theory and Methods*. Springer Science & Business Media.
- Cook, S. R., Gelman, A., and Rubin, D. B. (2006). Validation of software for Bayesian models using posterior quantiles. *Journal of Computational and Graphical Statistics*, 15(3):675–692.
- Cressie, N. (1989). Geostatistics. *The American Statistician*, 43(4):197–202.
- Dahlhaus, R. and Künsch, H. (1987). Edge effects and efficient parameter estimation for stationary random fields. *Biometrika*, 74(4):877–882.
- De Oliveira, V. and Han, Z. (2022). On information about covariance parameters in Gaussian Matérn random fields. *Journal of Agricultural, Biological and Environmental Statistics*, 27(4):690–712.
- Dietrich, C. R. and Newsam, G. N. (1997). Fast and exact simulation of stationary Gaussian processes through circulant embedding of the covariance matrix. *SIAM Journal on Scientific Computing*, 18(4):1088–1107.
- Frazier, D. T., Drovandi, C., and Kohn, R. (2023). Calibrated generalized Bayesian inference. *arXiv preprint arXiv:2311.15485*.
- Fuentes, M. (2007). Approximate likelihood for large irregularly spaced spatial data. *Journal of the American Statistical Association*, 102(477):321–331.
- Fuglstad, G.-A., Simpson, D., Lindgren, F., and Rue, H. (2019). Constructing priors that penalize the complexity of Gaussian random fields. *Journal of the American Statistical Association*, 114(525):445–452.

- Gelfand, A. E., Diggle, P., Guttorp, P., and Fuentes, M. (2010). *Handbook of Spatial Statistics*. CRC press.
- Geoga, C. J., Marin, O., Schanen, M., and Stein, M. L. (2023). Fitting Matérn smoothness parameters using automatic differentiation. *Statistics and Computing*, 33(2):48.
- Guillaumin, A. P., Sykulski, A. M., Olhede, S. C., and Simons, F. J. (2022). The debiased spatial Whittle likelihood. *Journal of the Royal Statistical Society Series B: Statistical Methodology*, 84(4):1526–1557.
- Guilleminot, J. (2020). Modeling non-Gaussian random fields of material properties in multiscale mechanics of materials. In *Uncertainty Quantification in Multiscale Materials Modeling*, pages 385–420. Woodhead Publishing.
- Guinness, J. and Fuentes, M. (2017). Circulant embedding of approximate covariances for inference from Gaussian data on large lattices. *Journal of Computational and Graphical Statistics*, 26(1):88–97.
- Guyon, X. (1982). Parameter estimation for a stationary process on a d-dimensional lattice. *Biometrika*, 69(1):95–105.
- Heyde, C. C. (1997). *Quasi-Likelihood and its Application: A General Approach to Optimal Parameter Estimation*. Springer.
- Hrafnkelsson, B. and Cressie, N. (2003). Hierarchical modeling of count data with application to nuclear fall-out. *Environmental and Ecological Statistics*, 10:179–200.
- Katzfuss, M. and Guinness, J. (2021). A general framework for Vecchia approximations of Gaussian processes. *Statistical Science*, 36(1):124 – 141.
- Kent, J. T. and Mardia, K. V. (1996). Spectral and circulant approximations to the likelihood for stationary Gaussian random fields. *Journal of Statistical Planning and Inference*, 50(3):379–394.
- Kleijn, B. and van der Vaart, A. (2012). The Bernstein-Von-Mises theorem under misspecification. *Electronic Journal of Statistics*, 6:354–381.
- Körner, T. W. (1988). *Fourier Analysis*. Cambridge University Press.
- Lindgren, F., Rue, H., and Lindström, J. (2011). An explicit link between Gaussian fields and Gaussian Markov random fields: the stochastic partial differential equation approach. *Journal of the Royal Statistical Society: Series B (Statistical Methodology)*, 73(4):423–498.
- Matheron, G. (1963). Principles of geostatistics. *Economic Geology*, 58(8):1246–1266.
- Matsuda, Y. and Yajima, Y. (2009). Fourier analysis of irregularly spaced data on R^d . *Journal of the Royal Statistical Society Series B: Statistical Methodology*, 71(1):191–217.

- Modrák, M., Moon, A. H., Kim, S., Bürkner, P., Huurre, N., Faltejsková, K., Gelman, A., and Vehtari, A. (2023). Simulation-based calibration checking for Bayesian computation: The choice of test quantities shapes sensitivity. *Bayesian Analysis*, 1(1):1–28.
- Monahan, J. F. and Boos, D. D. (1992). Proper likelihoods for Bayesian analysis. *Biometrika*, 79(2):271–278.
- Parzen, E. (1963). On spectral analysis with missing observations and amplitude modulation. *Sankhyā: The Indian Journal of Statistics, Series A (1961-2002)*, 25(4):383–392.
- Percival, D. B. and Walden, A. T. (1993). *Spectral Analysis for Physical Applications*. Cambridge University Press.
- Quiroz, M., Kohn, R., Villani, M., and Tran, M.-N. (2019). Speeding up MCMC by efficient data subsampling. *Journal of the American Statistical Association*, 114(526):831–843.
- Quiroz, M., Tran, M.-N., Villani, M., Kohn, R., and Dang, K.-D. (2021). The block-Poisson estimator for optimally tuned exact subsampling MCMC. *Journal of Computational and Graphical Statistics*, 30(4):877–888.
- Rasmussen, C. E. and Williams, C. K. (2006). *Gaussian Processes for Machine Learning*. MIT Press Cambridge, MA.
- Ribatet, M., Cooley, D., and Davison, A. C. (2012). Bayesian inference from composite likelihoods, with an application to spatial extremes. *Statistica Sinica*, 22(2):813–845.
- Rue, H. and Held, L. (2005). *Gaussian Markov Random Fields: Theory and Applications*. Chapman and Hall/CRC.
- Salomone, R., Quiroz, M., Kohn, R., Villani, M., and Tran, M.-N. (2020). Spectral subsampling MCMC for stationary time series. In *International Conference on Machine Learning*, pages 8449–8458. PMLR.
- Shao, X. and Wu, W. B. (2007). Asymptotic spectral theory for nonlinear time series. *The Annals of Statistics*, 35(4):1773–1801.
- Sidén, P., Lindgren, F., Bolin, D., Eklund, A., and Villani, M. (2021). Spatial 3D Matérn priors for fast whole-brain fMRI analysis. *Bayesian Analysis*, 16(4):1251–1278.
- Simons, F. J. and Olhede, S. C. (2013). Maximum-likelihood estimation of lithospheric flexural rigidity, initial-loading fraction and load correlation, under isotropy. *Geophysical Journal International*, 193(3):1300–1342.
- Sowell, F. (1989). A decomposition of block Toeplitz matrices with applications to vector time series. Unpublished manuscript available at <https://www.researchgate.net/profile/Fallaw-Sowell>.

- Stein, M. L., Chen, J., and Anitescu, M. (2013). Stochastic approximation of score function for Gaussian processes. *The Annals of Applied Statistics*, 7:1162–1191.
- Stroud, J. R., Stein, M. L., and Lysen, S. (2017). Bayesian and maximum likelihood estimation for Gaussian processes on an incomplete lattice. *Journal of Computational and Graphical Statistics*, 26(1):108–120.
- Sykulski, A. M., Olhede, S. C., Guillaumin, A. P., Lilly, J. M., and Early, J. J. (2019). The debiased whittle likelihood. *Biometrika*, 106(2):251–266.
- Tolbert, P. E., Mulholland, J. A., Macintosh, D. L., Xu, F., Daniels, D., Devine, O. J., Carlin, B. P., Klein, M., Butler, A. J., Nordenberg, D. F., et al. (2000). Air quality and pediatric emergency room visits for asthma and Atlanta, Georgia. *American Journal of Epidemiology*, 151(8):798–810.
- Van der Vaart, A. W. (2000). *Asymptotic Statistics*. Cambridge University Press.
- Varin, C., Reid, N., and Firth, D. (2011). An overview of composite likelihood methods. *Statistica Sinica*, 21:5–42.
- Vecchia, A. V. (1988). Estimation and model identification for continuous spatial processes. *Journal of the Royal Statistical Society: Series B (Methodological)*, 50(2):297–312.
- Villani, M., Quiroz, M., Kohn, R., and Salomone, R. (2024). Spectral subsampling MCMC for stationary multivariate time series with applications to vector ARTFIMA processes. *Econometrics and Statistics*, 32:98–121.
- White, H. (1982). Maximum likelihood estimation of misspecified models. *Econometrica*, 50(1):1–25.
- Whittle, P. (1954). On stationary processes in the plane. *Biometrika*, 41:434–449.